REPORT DOCUMENTATION PAGE	READ INSTRUCTIONS BEFORE COMPLETING FORM

1. REPORT NUMBER AFCRL-TR-75-0627	2. GOVT ACCESSION NO.	3. RECIPIENT'S CATALOG NUMBER

4. TITLE (and Subtitle)	5. TYPE OF REPORT & PERIOD COVERED
SOLAR MAGNETO-ATMOSPHERIC WAVES.	Scientific--Interim rept.
	6. PERFORMING ORG. REPORT NUMBER Scientific Report-1

7. AUTHOR(s)	8. CONTRACT OR GRANT NUMBER(s)
John H. Thomas, Alan H. Nye, and Alfred Clark, Jr.	F 19628-75-C-0011

9. PERFORMING ORGANIZATION NAME AND ADDRESS	10. PROGRAM ELEMENT, PROJECT, TASK AREA & WORK UNIT NUMBERS
Dept. of Mechanical and Aerospace Sciences University of Rochester Rochester, New York 14627	62101F, 678100 76490601

11. CONTROLLING OFFICE NAME AND ADDRESS	12. REPORT DATE
Air Force Cambridge Research Laboratories Hanscom AFB, Massachusetts 01731 Monitor/Steven Musman/LM	November 17, 1975
	13. NUMBER OF PAGES 71

14. MONITORING AGENCY NAME & ADDRESS(if different from Controlling Office)	15. SECURITY CLASS. (of this report)
	Unclassified
	15a. DECLASSIFICATION/DOWNGRADING SCHEDULE

16. DISTRIBUTION STATEMENT (of this Report)

Approved for public release, distribution unlimited.

17. DISTRIBUTION STATEMENT (of the abstract entered in Block 20, if different from Report)

18. SUPPLEMENTARY NOTES

19. KEY WORDS (Continue on reverse side if necessary and identify by block number)

Magneto-atmospheric waves
Running penumbral waves
Sunspots
Coronal disturbances
Hydromagnetic stability

20. ABSTRACT (Continue on reverse side if necessary and identify by block number)

The linearized theory of magneto-atmospheric waves (involving the combined restoring forces due to buoyancy, compressibility, and magnetic field) is developed for the case of a horizontal magnetic field which may vary with height. The convective stability of the basic atmosphere is considered, and it is shown that a nonuniform horizontal magnetic field may be destabilizing as well as stabilizing.

(OVER)

DD FORM 1473 1 JAN 73   EDITION OF 1 NOV 65 IS OBSOLETE

20. Abstract (continued)

A detailed model of a sunspot penumbra is studied in order to identify the mode of running penumbral waves. It is found that penumbral waves may be identified with magneto-atmospheric waves of the "plus" type that are vertically trapped at photospheric levels. Although most of the wave energy is contained in the penumbral photosphere and subphotosphere, the maximum vertical velocity occurs in the chromosphere where the waves are evanescent (and where they are observed in Hα).

An exact analytical solution for magneto-atmospheric wave modes is found in the case of an isothermal atmosphere permeated by a uniform horizontal magnetic field, without making the usual short-wavelength approximation. This solution is applied to an idealized model of the low-corona-chromosphere transition region as a model for flare-induced coronal waves. Disturbances propagate horizontally in the waveguide formed by the rapid density increase into the chromosphere below and the rapid increase in Alfvén speed into the corona above.

The exact solution mentioned above is also used in conjunction with a simple two-layer model of a sunspot penumbra to further study the mode of running penumbral waves. The lowest "plus" eigenmode of the model is in good agreement with observations of penumbral waves.

PERSONNEL

Air Force Contract F 19628-75-C-0011

John H. Thomas,   Principal Investigator

Alfred Clark, Jr., Faculty Associate

Alan H. Nye,   Research Assistant

3

CONTENTS

THE NATURE OF RUNNING PENUMBRAL WAVES

ALAN H. NYE* and JOHN H. THOMAS**

Max-Planck-Institut für Physik und Astrophysik, Munich, Germany

Abstract. A model of a sunspot penumbra, including the effects of magnetic field, compressibility, and buoyancy, is studied in order to identify the mode of running penumbral waves. It is found that the penumbral waves may be identified with gravity-modified magneto-acoustic waves of the 'plus' type that are vertically trapped at photospheric levels. Although most of the wave energy is contained in the penumbral photosphere and subphotosphere, the maximum vertical velocity occurs in the chromosphere where (i) the waves are evanescent and (ii) the vertical velocity is in fact observed (in Hα).

1. Introduction

Recent observations have disclosed an interesting pattern of velocity fields in sunspots. The most recent discovery is that of waves propagating radially outward in sunspot penumbrae (Zirin and Stein, 1972; Giovanelli, 1972). Zirin and Stein refer to these waves as running penumbral waves. With the further observations of Giovanelli (1974), we now have a fairly clear picture of the properties of these waves. The purpose of this theoretical paper is to study possible wave modes in a model of a sunspot penumbra in order to identify the mode of the running penumbral waves. We shall argue that the running penumbral waves are gravity-modified magneto-acoustic waves (of the 'plus' type) that are vertically trapped at photospheric levels.

Giovanelli (1974) has summarized the observations of running penumbral waves, and he presents the following picture. The waves are observed in Hα by means of their line-of-sight velocity. They occur in almost every sizable spot with a regular stable structure, but only rarely in active spots with complex structure. The waves travel outward in the penumbra at a typical speed of 15 km s^{-1}. The observed waves have periods in the range 180–240 s and horizontal wavelengths in the range 2350–3800 km. Observations near the limb have failed to reveal any horizontal motions associated with the penumbral waves, so the wave motion is predominantly vertical in Hα.

Thus far no detailed theoretical study of the mode of the running penumbral waves has appeared, although Moore (1973) has studied the related problem of the generation of penumbral waves in the umbra. Zirin and Stein (1972) tentatively identified the penumbral waves as sound waves, whereas Giovanelli (1972, 1974) identified them as Alfvén waves. The penumbral waves, with their predominant vertical motions, no doubt involve the combined effects of restoring forces due to compressibility, magnetic

---

* Also National Science Foundation Predoctoral Trainee, Dept. of Mechanical and Aerospace Sciences, University of Rochester, Rochester, N.Y., U.S.A.
** On leave of absence from the Dept. of Mechanical and Aerospace Sciences and the C. E. Kenneth Mees Observatory, University of Rochester, Rochester, N.Y., U.S.A.

field, and buoyancy, and a complete theory should account for all three effects. This is done in the present paper.

In studying penumbral waves, we face a difficulty, in that there seems to be no complete, generally accepted penumbral model on which to base our calculations. We have therefore constructed a penumbral model for use in studying wave modes. This model (presented in Section 3), while simple enough to permit analysis of wave modes, nevertheless reproduces all of the relevant features of penumbral structure, and is in reasonable quantitative agreement with observations. We have assumed the penumbral magnetic field to be purely horizontal, but varying with height. True penumbral magnetic fields are not purely horizontal, although they may be very nearly so (Nishi and Makita, 1973). There is some disagreement over the inclination of the magnetic field in a penumbra (see Beckers and Schröter (1969) for a summary of observations). The assumption of a horizontal field here is mostly a matter of convenience; the basic mechanism we propose for the vertical trapping of penumbral waves will also work for an inclined field. We have also taken our model to be horizontally uniform – that is, we have not tried to represent the horizontal filamentary structure of a penumbra or the radial geometry.

In Section 2 we present the basic equations for waves in our model penumbral atmosphere. The basic atmosphere is completely characterized in these equations by the vertical distribution of three parameters: the sound speed c, the Alfvén velocity v_A, and the local density scale height H. In order to illustrate the properties of the various wave modes that can occur, we study the dispersion relation that holds in the case of constant c, v_A, and H. In Section 3 we present the basic penumbral model in terms of the distributions of c, v_A, and H with height. In Section 4 we show that the penumbral waves may be identified with 'plus' modes that are trapped in the photospheric-subphotospheric region in our model. We discuss these modes further in Section 5.

2. Basic Equations and Dispersion Relations

In our simplified treatment of a sunspot penumbra we shall ignore the radial spreading of magnetic field lines, and consider the undisturbed magnetic field to be purely horizontal (in the x-direction) and varying with height z; i.e., $\mathbf{B}_0 = (B_0(z), 0, 0)$. We assume the field permeates an inviscid, perfectly conducting, plane stratified atmosphere with constant acceleration of gravity g ($=0.274$ km s^{-2}) in the negative z-direction. The undisturbed pressure, density, and temperature are denoted by $p_0(z)$, $\varrho_0(z)$, and $T_0(z)$, respectively. The atmosphere is in hydrostatic equilibrium, so that

$$\frac{\mathrm{d}}{\mathrm{d}z}\left(p_0 + \frac{B_0^2}{8\pi}\right) = -\varrho_0 g \,. \tag{1}$$

We then consider small adiabatic perturbations of this equilibrium atmosphere. We consider wave vectors only in the xz plane, and assume that the perturbation velocity $\mathbf{u} = (u, v, w)$ has the form $\mathbf{u} = \hat{\mathbf{u}} \exp i(k_x x - \omega t)$, with $\hat{\mathbf{u}} = \hat{\mathbf{u}}(z) = (\hat{u}(z), \hat{v}(z),$

$\hat{w}(z)$). Starting with the linearized equations of continuity, energy, and momentum, we can eliminate the pressure and density perturbations, and arrive at the set of three linearized momentum equations for the velocity components $\hat{u}$, $\hat{v}$, and $\hat{w}$, in which the basic atmosphere is completely described by the sound speed $c(z)$, the Alfvén velocity $v_A(z)$, and the local density scale height $H(z)$, defined by

$$c^2 = \left(\frac{\partial p_0}{\partial \varrho_0}\right)_s, \qquad v_A^2 = \frac{B_0^2}{4\pi\varrho_0}, \qquad \frac{1}{H} = -\frac{1}{\varrho_0}\frac{\partial \varrho_0}{\partial z}. \tag{2}$$

The linearized momentum equations are the following:

$$(\omega^2 - c^2 k_x^2)\,\hat{u} + i k_x c^2 \frac{d\hat{w}}{dz} - i k_x g \hat{w} = 0, \tag{3}$$

$$(\omega^2 - v_A^2 k_x^2)\,\hat{v} = 0, \tag{4}$$

$$(c^2 + v_A^2)\frac{d^2\hat{w}}{dz^2} + \left[\frac{d}{dz}(c^2 + v_A^2) - \frac{c^2 + v_A^2}{H}\right]\frac{d\hat{w}}{dz} + (\omega^2 - v_A^2 k_x^2)\,\hat{w} +$$
$$+ i k_x \left[\frac{dc^2}{dz} - \frac{c^2}{H} + g\right]\hat{u} + i k_x c^2 \frac{d\hat{u}}{dz} = 0. \tag{5}$$

We can eliminate the horizontal velocity components $\hat{u}$ and $\hat{v}$ from the system of Equations (3)–(5) to obtain a single equation for the vertical velocity $\hat{w}$, in the form

$$\frac{d^2\hat{w}}{dz^2} + A(z)\frac{d\hat{w}}{dz} + B(z)\,\hat{w} = 0, \tag{6}$$

where

$$A(z) = -\frac{1}{H} + \left[\frac{\omega^4}{(\omega^2 - c^2 k_x^2)}\frac{dc^2}{dz} + (\omega^2 - c^2 k_x^2)\frac{dv_A^2}{dz}\right] \times$$
$$\times \left[v_A^2(\omega^2 - c^2 k_x^2) + c^2\omega^2\right]^{-1} \tag{7}$$

and

$$B(z) = \left[(\omega^2 - v_A^2 k_x^2)(\omega^2 - c^2 k_x^2) - g\left(g - \frac{c^2}{H}\right)k_x^2 -\right.$$
$$\left. - g \times \frac{\omega^2 k_x^2}{(\omega^2 - c^2 k_x^2)}\frac{dc^2}{dz}\right]\left[v_A^2(\omega^2 - c^2 k_x^2) + c^2\omega^2\right]^{-1}. \tag{8}$$

With the transformation

$$\phi(z) = \hat{w}(z)\exp\left[\tfrac{1}{2}\int_0^z A(z)\,dz\right] \tag{9}$$

Equation (6) assumes the form

$$\frac{d^2\phi}{dz^2} + f(k_x, \omega; z)\,\phi = 0, \tag{10}$$

7

where

$$f = B - \tfrac{1}{4}A^2 - \tfrac{1}{2}\frac{dA}{dz}. \tag{11}$$

Here, $|\phi|^2$ is roughly proportional to the kinetic energy of wave motion. Equation (10) is the propagation equation for waves in an atmosphere with vertically varying c^2, v_A^2, and H. For given distributions of $c^2(z)$, $v_A^2(z)$, and $H(z)$, we can use the expression for $f(z)$ (Equation (11)) to distinguish roughly between local regions where a wave with a particular frequency ω and horizontal wavelength k_x is vertically propagating ($f > 0$) or vertically evanescent ($f < 0$). We shall use this approach for our penumbral model in Section 4.

The simplest case to study is that of constant c^2, v_A^2, and H. We shall consider this case now in order to show the kinds of wave modes which can occur. Although this case does not apply strictly to a real penumbra, or in fact to our penumbral model, we can nevertheless apply the resulting dispersion relation locally to get an approximate picture of the wave modes. We can also approximate a continuous vertical variation of the parameters in the penumbra by a series of layers in which they are constant. In the case of constant c^2, v_A^2, and H, Equations (3)–(5) have constant coefficients, and we can assume a solution of the form $\hat{\mathbf{u}}(z) = \bar{\mathbf{u}}\exp(ik_z z + z/2H)$, where $\bar{\mathbf{u}} = (\bar{u}, \bar{v}, \bar{w})$ is a constant vector. Here, the factor $\exp(z/2H)$ accounts for the fact that, to conserve energy, the perturbation amplitude must grow as the density decreases. The system of Equations (3)–(5) then becomes (cf., Yu, 1965):

$$(\omega^2 - c^2 k_x^2)\,\bar{u} + ik_x\left[ik_z c^2 - \left(g - \frac{c^2}{2H}\right)\right]\bar{w} = 0, \tag{12}$$

$$(\omega^2 - v_A^2 k_x^2)\,\bar{v} = 0, \tag{13}$$

$$ik_x\left[ik_z c^2 + \left(g - \frac{c^2}{2H}\right)\right]\bar{u} + \left[(\omega^2 - v_A^2 k_x^2) - (c^2 + v_A^2)\times\right.$$
$$\left.\times\left(k_z^2 + \frac{1}{4H^2}\right)\right]\bar{w} = 0. \tag{14}$$

The dispersion relation for waves is obtained from the condition for nonzero solutions of the homogeneous system (12)–(14), i.e., the vanishing of the determinant of the coefficients. This yields the dispersion relation

$$(\omega^2 - v_A^2 k_x^2)\left\{\omega^4 - (c^2 + v_A^2)\left(k_x^2 + k_z^2 + \frac{1}{4H^2}\right)\omega^2 + \right.$$
$$\left. + c^2 v_A^2 k_x^2\left(k_x^2 + k_z^2 + \frac{1}{4H^2}\right) - g\left(g - \frac{c^2}{H}\right)k_x^2\right\} = 0. \tag{15}$$

We now discuss the various wave modes given by this dispersion relation, with some comments on their relation to running penumbral waves.

8

2.1. THE PURE ACOUSTIC MODE

The dispersion relation (15) is satisfied with $\omega^2 = c^2 k_x^2$ for the particular imaginary value of k_z given by $ik_z = (1/2H) - (g/c^2)$. From Equations (12)–(14) we see the corresponding motion has $\bar{u} \neq 0$, whereas $\bar{v} = \bar{w} = 0$. This mode is thus a purely compressional, acoustic mode with dispersion relation identical to that of a homogeneous isothermal gas. This can occur since the motion is horizontal and parallel to the magnetic field, and thus there is no contribution from buoyant or magnetic forces. The amplitude behaves as

$$\hat{u} = \bar{u} \exp\left[\left(\frac{1}{H} - \frac{g}{c^2}\right) z\right],$$

and thus grows exponentially with height (since $H < c^2/g$ for stability of the unperturbed atmosphere (Yu, 1965)). The total momentum and energy are finite, however, provided there is a lower boundary confining the motion to a semi-infinite range of z. This mode is identical to the Lamb mode in the non-magnetic case, except that here the scale height H is modified by the magnetic field. Since this mode has no vertical motion, it can not be associated with the running penumbral waves.

2.2. THE PURE ALFVÉN MODE

A root of the dispersion relation (15), for arbitrary k_z, is given by $\omega^2 = v_A^2 k_x^2$, which is the same as the dispersion relation for a pure Alfvén wave in a homogeneous atmosphere with uniform magnetic field. With $\omega^2 = v_A^2 k_x^2$, however, the other factor in the dispersion relation (15) is in general not zero, and thus Equations (12)–(14) show that the motion has $\bar{v} \neq 0$, whereas $\bar{u} = \bar{w} = 0$. The motion is purely horizontal and purely transverse to the magnetic field. Thus, the pure Alfvén mode in a stratified atmosphere is, so to speak, plane polarized, with no vertical motions. With $\bar{w} = 0$ there is no contribution from the buoyancy force, and, further, with $\bar{u} = 0$ the motion is incompressible, so the wave behaves as a pure Alfvén wave (with the amplitude factor $\exp(z/2H)$). Again, since this mode has no vertical motions, it can not be associated with the running penumbral waves. We turn now to the remaining roots of the dispersion relation (15), which do permit vertical motions.

2.3. THE PLUS AND MINUS MODES

The remaining roots of the dispersion relation (15) are given by

$$\omega_\pm^2 = \tfrac{1}{2}\left\{(c^2 + v_A^2)\left(k_x^2 + k_z^2 + \frac{1}{4H^2}\right) \pm \left[(c^2 + v_A^2)^2\left(k_x^2 + k_z^2 + \frac{1}{4H^2}\right)^2 - \right.\right.$$
$$\left.\left. - 4c^2 v_A^2 k_x^2\left(k_x^2 + k_z^2 + \frac{1}{4H^2}\right) + 4g\left(g - \frac{c^2}{H}\right)k_x^2\right]^{1/2}\right\}. \quad (16)$$

We shall refer to these two modes as the 'plus' and 'minus' modes. These modes involve the interaction of all three restoring forces: buoyant, pressure, and magnetic.

9

They reduce to more familiar wave modes in certain limiting cases. For example, in the limit of vanishing magnetic field ($v_A \to 0$) they reduce to the acoustic and gravity modes of an isothermal atmosphere (see, for example, Thomas *et al.*, 1971). Alternatively, in the limit of no stratification ($H \to \infty$, $g \to 0$), they reduce to the fast and slow magnetoacoustic waves in a homogeneous atmosphere (see, for example, Osterbrock, 1961). For intermediate cases (such as for penumbral conditions), we can look at the modes as being either magnetically modified acoustic-gravity waves or gravity-modified magnetoacoustic waves. We shall continue to use the terms plus and minus modes here.

The plus and minus modes, for $k_z = 0$, are shown schematically in a diagnostic diagram in Figure 1. The asymptotic behavior of the dispersion relation (16) for $k_z = 0$ is such that

$$\omega_+^2 \to \frac{c^2 + v_A^2}{4H^2}, \qquad \omega_-^2 \to 0 \quad \text{for} \quad k_x \to 0, \tag{17}$$

and

$$\omega_+^2 \to k_x^2 \max(c^2, v_A^2), \quad \omega_-^2 \to k_x^2 \min(c^2, v_A^2) \quad \text{for} \quad k_x \to \infty. \tag{18}$$

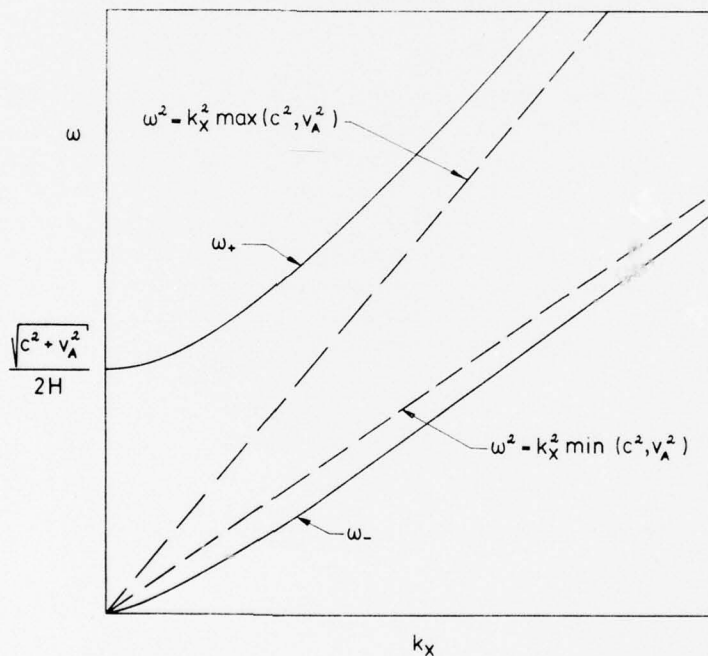Fig. 1. Schematic diagnostic diagram of the plus and minus modes, showing curves for $k_z = 0$ (solid lines). The plus mode has a finite cutoff frequency as $k_x \to 0$. For $k_x \to \infty$, the plus and minus modes approach the dispersion lines for the pure acoustic and pure Alfvén modes. For strong stratification and weak magnetic field, the minus mode approaches the line $\omega = k_x v_A$ from above rather than below.

In the diagnostic diagram (Figure 1), there are vertically-propagating waves ($k_z^2 > 0$) above the ω_+ curve and below the ω_- curve, and evanescent waves ($k_z^2 < 0$) in the region between the two curves.

The plus mode has a finite cutoff frequency of $(\omega_+)_c = (c^2 + v_A^2)^{1/2}/2H$ as $k_x \to 0$. Estimates of this cutoff frequency at photospheric levels in a penumbra give values just a little lower than the frequencies of penumbral waves. This suggests that the penumbral waves might be identified with plus modes. We shall show this in more detail through the use of our penumbral model.

3. The Penumbral Model

We now present the penumbral model to be used in our wave calculations. For our purposes, a penumbral model consists of specified distributions of c^2, v_A^2, and H with height z. To simplify the calculations, we have chosen to represent the expected vertical variation of these parameters by piecewise linear functions. The specified forms of $c^2(z)$, $v_A^2(z)$, and $H(z)$ are shown in Figure 2. The important features of the model are as follows. The sound speed increases with depth into the convection zone from a broad minimum in the penumbral photosphere and chromosphere. The Alfvén velocity increases rapidly with height due to the nearly exponential decrease of density while the magnetic field decreases nearly linearly. The density scale height increases on either side of a minimum in the penumbral photosphere and low chromosphere. The model thus reproduces the main expected features of vertical penumbral structure. The numerical values of the parameters were chosen to represent a typical penumbra.

The distribution of the sound speed was determined primarily from the expected temperature distribution. Kjeldseth Moe and Maltby (1969) report that the temperature T in the penumbra may be obtained by adding a constant $\Delta\theta = 0.055$ to the θ values of the quiet photosphere, where $\theta = 5040/T$. With this $\Delta\theta$, the calculated relative intensities averaged over the penumbral fine structure agreed well with observations. Kjeldseth Moe and Maltby used the Bilderberg Continuum Atmosphere (Gingerich and de Jager, 1968) for their quiet photospheric temperatures; here, we use the more recent Harvard-Smithsonian Reference Atmosphere (HSRA, Gingerich et al., 1971). Using the constant $\Delta\theta = 0.055$, the penumbral temperature minimum is found to be 3989 K, yielding a minimum value of the sound speed squared of $c^2 = 43.5$ km^2 s^{-2}. The slope of the linear increase of c^2 into the convection zone was taken to be 0.1 km s^{-2}; this choice is also based on the behavior of the HSRA. The distribution of sound speed (in km s^{-1}) is given by

$$c^2(z) = \begin{cases} 63.5 - 0.1z & z \leqslant 200 \\ 43.5 & z > 200. \end{cases} \tag{19}$$

At some point in the penumbral chromosphere the sound speed will increase rapidly to coronal values. However, this increase takes place above the region where the penumbral waves are trapped in our model, so we have not included this in the model.
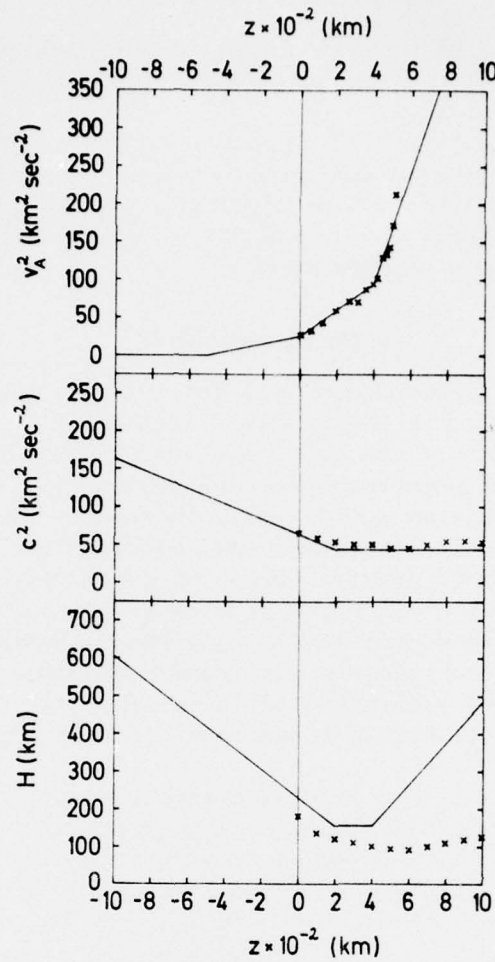
11

Fig. 2.   Distribution of c^2, v_A^2, and H with height z in the penumbral model (solid lines). The data (crosses) for v_A^2 are based on penumbral observations (see text). Data points for quiet photospheric values of c^2 and H, based on the HSRA, are shown only for comparison with the penumbral model.

The distribution of c^2 is shown in Figure 2, along with quiet atmospheric values of c^2 from the HSRA (Nakagawa, 1973) for comparison.

To determine the Alfvén velocity, we assumed that the magnetic field strength decreases linearly with height and is 1000 G at $z=0$. The rate of decrease of field strength with height was taken to be 0.2 G km^{-1}, in accordance with observations (see Bray and Loughhead, 1964). The photospheric densities were estimated from the penumbral model of Makita (1963), the only penumbral model to give densities. His densities are consistent with more recent quiet photospheric models. The resulting

12

values of v_A^2 are plotted in Figure 2. The vertical distribution of these points was approximated in our model by two straight-line segments, with the upper segment extrapolated to greater heights. In the convection zone, the Alfvén velocity was approximated by another straight line segment which goes to zero at $z = -500$ km, due primarily to the increase in density with depth, but also to the fact that the penumbral field probably lies over the convection zone. The resulting distribution of the Alfvén velocity (in km s^{-1}) is given by

$$v_A^2(z) = \begin{cases} 0 & z < -500 \\ 25 + 0.05z & -500 \leqslant z < 0 \\ 25 + 0.172z & 0 \leqslant z \leqslant 400 \\ 94 + 0.75\,(z - 400) & z > 400. \end{cases} \tag{20}$$

The distribution of the local density scale height H (in km) with height was chosen to be

$$H(z) = \begin{cases} 230 - 0.375z & z < 200 \\ 155 & 200 \leqslant z < 400 \\ 155 + 0.55\,(z - 400) & z \geqslant 400. \end{cases} \tag{21}$$

In choosing values for H, we were guided by the following expression for the vertical entropy gradient in the atmosphere:

$$\frac{ds}{dz} = \frac{\varrho c_v \kappa}{\beta T}\left[\left(c^2 + \frac{v_A^2}{2}\right)\frac{1}{H} - g - \frac{d}{dz}\left(\frac{v_A^2}{2}\right)\right], \tag{22}$$

where c_v is the specific heat at constant volume, κ is the isothermal compressibility, and β is the coefficient of thermal expansion. This relation follows from the hydrostatic equation (1) and the basic thermodynamic relation

$$T\,ds = \frac{\kappa c_v}{\beta}\,(dp - c^2\,d\varrho). \tag{23}$$

The distribution of H given in (21) is such that the entropy gradient ds/dz is negative in the upper convection zone and positive in the penumbral photosphere and chromosphere. The distribution of H is shown in Figure 2, along with quiet atmospheric values of H from the HSRA (Nakagawa, 1973) for comparison. Here we can see the effect of the supporting magnetic field; the scale height is greater in the penumbra than in the quiet atmosphere. The effect of the magnetic field increases as the density decreases.

4. Trapping of Plus Modes in the Penumbral Photosphere

We now show that the running penumbral waves can be identified in our model with plus modes that are vertically trapped at photospheric levels. The basic mechanism for the trapping is the refraction due to (i) the increasing Alfvén velocity with increasing height in the photosphere-low chromosphere, and (ii) the increasing sound speed with depth in the convection zone. We shall demonstrate the trapping mechanism in two

13

ways: first, by considering the local dispersion relation (16) at three distinct levels in the model penumbra (assuming locally constant parameters), and second, by considering the propagation equation (10) for the complete continuous penumbral model (Figure 2).

4.1. THREE-LEVEL MODEL

A convenient method of looking at wave modes in our model is to draw diagnostic diagrams such as Figure 1 for various heights in the atmosphere, assuming locally constant values of c^2, v_A^2, and H – that is, ignoring the derivatives of these parameters in Equation (3)–(5). Although only approximate, this method does give some feeling for the behavior of the wave modes. We shall draw diagnostic diagrams for three different levels in our model penumbra; one in the convection zone, one in the photosphere, and one in the chromosphere. We may interpret these diagnostic
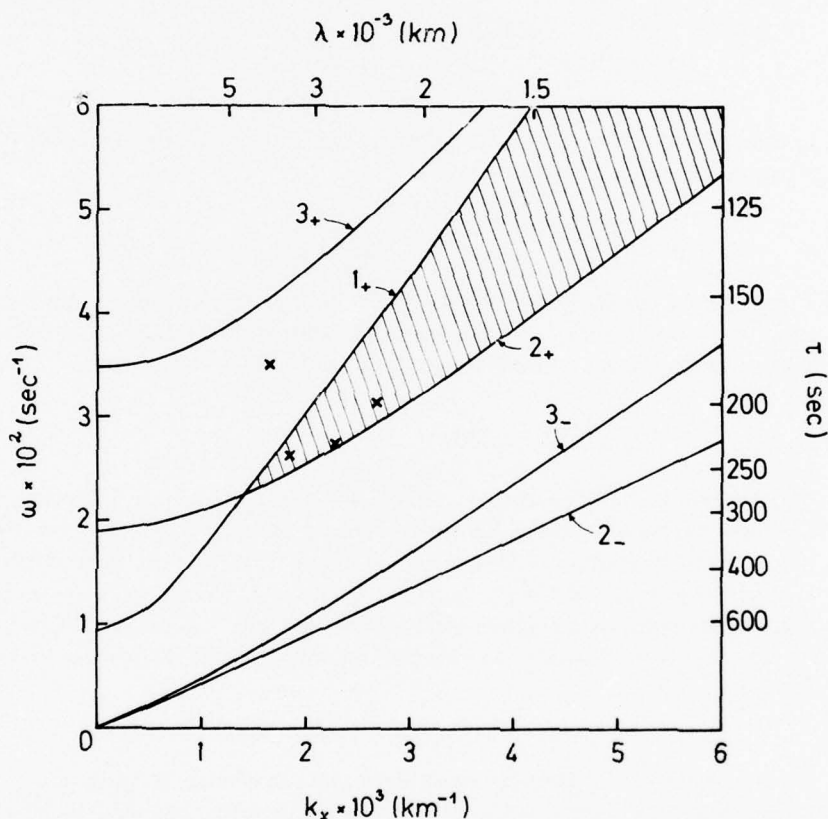

Fig. 3. Superimposed diagnostic diagrams for values of c^2, v_A^2, and H at three different levels in the model penumbra: level, 1 $z = -1400$ km; level 2, $z = -50$ km; level 3, $z = 500$ km. The shaded region is a region of vertical trapping of plus modes around level 2. The crosses correspond to observed running penumbral waves (Giovanelli, 1974).

14

diagrams more properly as representing a three-layer model of the penumbra, where in each layer the parameters are constant. A middle layer of finite thickness representing the penumbral photosphere is bounded above and below by semi-infinite layers representing the penumbral chromosphere and convection zone, respectively.

Figure 3 shows diagnostic diagrams for values of c^2, v_A^2, and H at three different levels in the penumbral model: $z \approx -1400$ km (layer 1, convection zone), $z = -50$ km (layer 2, penumbral photosphere), and $z = 500$ km (layer 3, penumbral chromosphere). The important feature of this figure is the existence of the shaded region in which the plus modes are vertically propagating in layer 2, but are vertically evanescent in layers 1 and 3. These modes are thus trapped in layer 2. The plus mode diagnostic curve for layer 3 lies above that of layer 2 because of the higher Alfvén velocity in layer 3. For higher levels in the chromosphere, the plus mode curve for layer 3 will be higher than that shown. The plus mode diagnostic curve for layer 1 has a lower cutoff frequency than layer 2 due to the larger scale height in the convection zone, but lies above the curve for layer 2 for higher values of k_x because of the higher value of c^2 in layer 1. For deeper levels in the convection zone, the plus mode curve for layer 1 will have an even lower cutoff frequency and a steeper slope. The existence of the region of trapping in the diagnostic diagram is a consequence of the qualitative features of our model and is not dependent on the particular choice of numerical values.

There is no trapping of minus modes in Figure 3. All the minus modes propagating in layer 2 are also propagating in layer 3. The minus mode curve for layer 1 has vanished since the Alfvén velocity is zero and the atmosphere is convectively unstable at that level.

Also shown in Figure 3 are four data points corresponding to penumbral waves observed in different sunspots by Giovanelli (1974) for which he gives specific wavelength and periods. These points tend to cluster in the long-wavelength end of the shaded region of trapping of the plus modes. The one point which lies outside the shaded region does lie in the region of trapping if the parameter values in layer 1 are chosen to represent a lower level in the convection zone. That is, a wave of this frequency and wavelength is reflected at a lower level in the convection zone in our model. This data point is considered atypical by Giovanelli, however. The observational data correspond to different sunspots, no doubt having different field strengths, whereas the diagnostic curves are for a single choice of the model parameters. Nevertheless, the resulting picture in Figure 3 clearly shows that the running penumbral waves should be identified with plus modes which are vertically trapped at photospheric levels in our model.

4.2. CONTINUOUS MODEL

We now illustrate more accurately the trapping of the penumbral waves by making use of our complete penumbral model (Figure 2) in conjunction with the propagation equation (10). Roughly speaking, a wave is vertically propagating when the function $f(k_x, \omega; z)$ (Equation (11)) is positive, and is vertically evanescent when f is negative. In Figure 4 we have plotted f as a function of z for our penumbral model (Figure 2) for
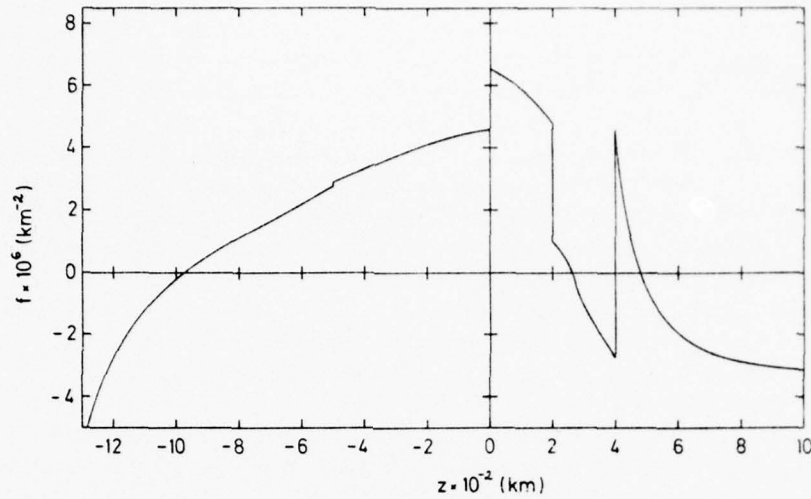
15

Fig. 4.   The function $f(k_x, \omega; z)$ evaluated for the penumbral model (Figure 2) with $k_x = 2 \times 10^{-3}$ km^{-1}, $\omega = 3 \times 10^{-2} \text{ s}^{-1}$.

a typical value of horizontal wavenumber $(k_x = 2 \times 10^{-3} \text{ km}^{-1})$ and frequency $(\omega = 3 \times 10^{-2} \text{ s}^{-1})$ for penumbral waves. The function $f(z)$ is discontinuous due to the discontinuities in the first derivatives of the parameters c^2, v_A^2, and H in our model. The general behavior of f is that it is positive in a central region extending from $z \approx -1000$ km to roughly $z \approx 300$ km, and negative above and below this region.

In the lowest order WKB approximation, the general solution to (10) is given by

$$\phi(z) = \exp\left[\pm i \int_0^z \sqrt{f}\, \mathrm{d}z\right]. \tag{24}$$

If f is positive for $0 < z < z_0$ and negative for $z > z_0$, then the solution for $z > z_0$ which is bounded as $z \to \infty$ can be written as

$$\phi(z) = \exp\left[\pm i \int_0^{z_0} \sqrt{f}\, \mathrm{d}z - \int_{z_0}^z \sqrt{-f}\, \mathrm{d}z\right]. \tag{25}$$

Thus, for $z > z_0$, the solution has the form of an exponential decay (with variable exponential factor), and the wave may be characterized as evanescent in the vertical direction. This analysis is somewhat crude, however, since the WKB solution (24) is not accurate in the neighborhood of z_0. The same analysis applies to the case where f is positive for $-z_0' < z < 0$ and negative for $z < -z_0'$. The wave then becomes evanescent as z decreases below $-z_0'$. Applying this to Figure 4, we conclude that a wave with the specified horizontal wavelength and frequency is trapped roughly in the

16

central region $-1000 < z < 300$ where f is positive. The exact location of the upper boundary of the trapping region is somewhat unclear due to the complicated discontinuous behavior of f there. This is due to the piecewise linear nature of our model; with smoother distributions of c^2, v_A^2, and H, the function f would have a single, smooth zero crossing at some $z > 0$.

We have been discussing the behavior of the function $\phi(z)$. Comparison with the case of constant parameters shows that $|\phi|^2$ is roughly proportional to the kinetic energy of vertical motion of the wave ($\phi \sim \sqrt{\varrho} \, w$). Thus, it is the kinetic energy that is trapped in the region of positive f. The amplitude of the vertical velocity behaves somewhat differently. From Equations (9) and (25) we have, for $z > z_0$,

$$\hat{w}(z) = \exp\left[\pm i \int_0^{z_0} \sqrt{f} \, \mathrm{d}z + Q(z) \right], \tag{26}$$

where

$$Q(z) = -\tfrac{1}{2} \int_0^z A \, \mathrm{d}z - \int_{z_0}^z \sqrt{-f} \, \mathrm{d}z. \tag{27}$$

The function $A(z)$ (Equation (7)) is negative over a range in z, and the function $Q(z)$ will remain positive over a range of z beyond z_0 before becoming negative. Thus, the vertical velocity continues to increase above z_0 before reaching a maximum at $z = z_1$, where z_1 is determined from the relation $Q(z_1) = 0$. This can occur in spite of the decreasing energy above $z = z_0$ due to the rapid decrease in density.

By numerically evaluating the integrals in (27), we have estimated the point z_1 of maximum vertical velocity in our model, again for the choice $k_x = 2 \times 10^{-3} \ \mathrm{km}^{-1}$ and $\omega = 3 \times 10^{-2} \ \mathrm{s}^{-1}$. The resulting value is $z_1 \approx 1250$ km. This is at a level where the wave is evanescent, and is well into the region of formation of Hα (Vernazza *et al.*, 1973). Thus, although the trapped waves have their maximum energy at lower levels ($z \approx 0$) where the density is higher, the vertical velocity is greatest at chromospheric levels where is it observed.

5. Discussion

An important conclusion that emerges from our model is that the running penumbral waves are basically a photospheric phenomenon, even though they are observed at chromospheric levels. This is really an expected result; the phase velocity of the penumbral waves is typical of photospheric conditions rather than chromospheric. For example, the Alfvén velocity at Hα levels in the penumbra is far greater than the phase velocity of the penumbral waves. In our picture, the waves are evanescent where they are observed. That is, the observed vertical motions are a passive response to an actively propagating wave at lower levels. We have shown that although the energy is trapped at photospheric levels, the vertical velocity reaches its maximum value at levels of formation of Hα, consistent with observations.

The concept of the penumbral waves as a photospheric phenomenon is also quite

17

consistent with their expected source of excitation. Moore (1973) has shown that the likely source of excitation of the penumbral waves is oscillatory convection in a sub-photospheric layer in the umbra. The observation that the penumbral waves disappear suddenly at the boundary between the white-light penumbra and the surrounding photosphere also supports the photospheric nature of the waves. In the chromosphere, the penumbral fibril structure extends outward beyond this boundary.

The basic mechanism for the vertical trapping of the penumbral waves is not sensitive to the details of our penumbral model. This mechanism is based primarily on the increase in the sound speed as we go down into the convection zone and the increase in the Alfvén velocity as we go up into the chromosphere. These features are certain to remain in any improved penumbral model. Observationally, the insensitivity of the basic mechanism is confirmed by the fact that penumbral waves are seen in almost every stable, regular sunspot (Zirin and Stein, 1972).

The character of the trapped plus modes is different at different heights. The wave is more nearly acoustic at low levels (convection zone), but is more nearly Alfvénic at higher levels (photosphere and low chromosphere). The effect of stratification and gravity, while not dominant, is felt throughout the trapping region.

Although we have not attempted to calculate them, there are certainly resonant modes in our model which arise from the constructive interference of plus modes reflected from above and below in the trapping region. The resonant dispersion curves would lie in the shaded region in Figure 3. However, since the penumbral waves are a somewhat transitory phenomenon, there is no reason to associate them specifically with such a resonant mode; it is sufficient that a wave of the proper frequency and horizontal wavelength be vertically trapped.

Since our penumbral model is horizontally uniform, it cannot account for any observed horizontal (radial) variations in the penumbral waves. We can roughly account for the radial geometry of the penumbra by noting that the energy in a vertically trapped wave will decrease as $1/r$, where r is radius measured from the spot center, as the wave propagates radially outward. This accounts at least in part for the observed decrease in wave amplitude with radius. The sudden disappearance of the waves at the outer edge of the penumbra is associated with the more fundamental problem of the basic existence of the sharp boundary between the white-light penumbra and the surrounding photosphere.

Finally, we should note that our assumption of adiabatic perturbations is invalid over a limited range of height in the low photosphere, say the first few hundred kilometers above $z = 0$. Here one should account for the rapid radiative exchange. The main effect of the radiative transfer on the plus modes is to effectively replace the adiabatic sound speed in this limited region by something nearer to the isothermal sound speed. The overall effect on the trapped plus modes discussed here will be quite small, even quantitatively.

Acknowledgements

References

Beckers, J. M. and Schröter, E. H.: 1969, *Solar Phys.* **10**, 384.

Bray, R. J. and Loughhead, R. E.: 1964, *Sunspots*, Chapman and Hall, London, pp. 212–214.

Gingerich, O. and de Jager, C.: 1968, *Solar Phys.* **3**, 5.

Gingerich, O., Noyes, R. W., Kalkofen, W., and Cuny, Y.: 1971, *Solar Phys.* **18**, 347.

Giovanelli, R. G.: 1972, *Solar Phys.* **27**, 71.

Giovanelli, R. G.: 1974, in R. Grant Athay (ed.), 'Chromospheric Fine Structure', *IAU Symp.* **56**, 137.

Kjeldseth Moe, O. and Maltby, P.: 1969, *Solar Phys.* **8**, 275.

Makita, M.: 1963, *Publ. Astron. Soc. Japan* **15**, 145.

Moore, R. L.: 1973, *Solar Phys.* **23**, 403.

Nakagawa, Y.: 1973, *Solar Phys.* **33**, 87.

Nishi, K. and Makita, M.: 1973, *Publ. Astron. Soc. Japan* **25**, 51.

Osterbrock, D. E.: 1961, *Astrophys. J.* **134**, 347.

Thomas, J. H., Clark, P. A., and Clark, A., Jr.: 1971, *Solar Phys.* **16**, 51.

Vernazza, J. E., Avrett, E. H., and Loeser, R.: 1973, *Astrophys. J.* **184**, 605.

Yu, C. P.: 1965, *Phys. Fluids* **8**, 650.

Zirin, H. and Stein, A.: 1972, *Astrophys. J.* **173**, L85.

Convective instability in the presence of a nonuniform horizontal magnetic field

John H. Thomas* and Alan H. Nye*

Max-Planck-Institut für Physik und Astrophysik, München, Federal Republic of Germany
(Received 14 August 1974; final manuscript received 6 December 1974)

Newcomb's criterion for convective stability in the presence of a horizontal magnetic field is written in a form which explicitly shows the effect of vertical variations of the magnetic field strength. It is shown that a nonuniform horizontal magnetic field can be *destabilizing* as well as stabilizing.

We consider the convective instability of a compressible, inviscid, perfectly conducting gas permeated by a horizontal magnetic field $\mathbf{B} = [B(z), 0, 0]$ that may vary with height z, under a uniform gravitational acceleration g (in the negative z direction), assuming adiabatic perturbations. The first complete treatment of this problem was given by Newcomb[1] using the energy integral method. He showed that a necessary and sufficient condition for stability is given by

$$-\frac{d\rho}{dz} > \frac{\rho^2 g}{\gamma p} \ , \tag{1}$$

where ρ is mass density, p is pressure, and γ is the ratio of specific heats. In the case of instability, the most unstable mode has the form of an interchange of long but finite segments of magnetic field lines. The stability criterion (1) was also derived by Yu[2] by considering the force balance on a displaced magnetic flux tube.

Newcomb noted that the critical density gradient on the right-hand side of (1) is, at least explicitly, independent of the magnetic field, and is, in fact, that given by the Schwarzschild criterion[3] in the absence of a magnetic field. However, in the case of a nonuniform horizontal magnetic field (for which Newcomb's analysis is valid), the static distribution of pressure and density is affected by the magnetic field, and thus the stability criterion (1) depends implicitly on the magnetic field. This point, which was overlooked by Newcomb, will be pursued here.

Using the equation of hydrostatic equilibrium,

$$\frac{d}{dz}\left(p + \frac{B^2}{8\pi} \right) = -\rho g \ , \tag{2}$$

and the equation of state of a perfect gas, $p = \rho R T$, the stability criterion (1) can be written in the form

$$\frac{dT}{dz} - \left(\frac{dT}{dz}\right)_s > -\frac{1}{\rho R}\frac{d}{dz}\left(\frac{B^2}{8\pi}\right) \ , \tag{3}$$

where $(dT/dz)_s = -g/c_p = -g(\gamma-1)/\gamma R$ is the adiabatic temperature gradient. The new form (3) of the stability criterion has an advantage over the form (1) in that it shows *explicitly* the effect of vertical variations of the magnetic field, since the temperature distribution is independent of the magnetic field. For a uniform magnetic field ($B = $ const), (3) reduces to

$$\frac{dT}{dz} - \left(\frac{dT}{dz}\right)_s > 0,$$

which is identical to the Schwarzschild criterion in the absence of a magnetic field. [Note that usually, e.g., in a star, dT/dz and $(dT/dz)_s$ are both negative.] Thus, a uniform horizontal magnetic field has no effect on the condition for the onset of convective instability,[4] although, as Newcomb[1] also showed, it does have an effect on the growth rates of unstable modes.

If, however, the magnetic field is nonuniform, then (3) shows that the field can be stabilizing (in the case $dB/dz > 0$) or destabilizing ($dB/dz < 0$). A field that increases with height ($dB/dz > 0$) can stabilize the atmo-

20

sphere in the presence of a superadiabatic temperature gradient. When the field decreases with height ($dB/dz < 0$), the critical temperature gradient is reduced below the adiabatic gradient.

As an illustration of the destabilizing effect for $dB/dz < 0$, consider the case of an isothermal atmosphere, which is convectively stable in the absence of a magnetic field. The stability criterion (3) reduces to

$$-\frac{1}{\rho}\frac{d}{dz}\left(\frac{B^2}{8\pi}\right) < -R\left(\frac{dT}{dz}\right)_s = g\left(\frac{\gamma-1}{\gamma}\right) . \qquad (4)$$

If the magnetic pressure decreases more rapidly with height than the critical rate

$$\left[\frac{d}{dz}\left(\frac{B^2}{8\pi}\right)\right]_c = -\rho g\left(\frac{\gamma-1}{\gamma}\right) , \qquad (5)$$

the atmosphere will be convectively unstable. For this critical magnetic field gradient, the corresponding pressure gradient is found from (2) to be

$$\left[\frac{dp}{dz}\right]_c = -\frac{\rho g}{\gamma} . \qquad (6)$$

Thus, in the state of marginal stability in an isothermal atmosphere, the gradient of gas pressure balances the fraction $1/\gamma$ of the gravitational force, while the gradient of magnetic pressure balances the remaining fraction $(\gamma-1)/\gamma$ of the gravitational force.

A special case of interest is that of an isothermal atmosphere in which the field decreases with height in just the manner that causes the Alfvén speed $v_A = (B^2/4\pi\rho)^{1/2}$ to remain constant. In this case, (4) can be written as

$$\frac{v_A^2}{c^2} < 2\left(\frac{\gamma-1}{\gamma}\right) , \qquad (7)$$

where $c = (\gamma RT)^{1/2}$ is the adiabatic sound speed. This stability criterion was obtained for this special case by Yu[5] from a normal mode analysis. Parker[6] has studied this case, including the effect of cosmic-ray pressure, in connection with the gaseous disk of the galaxy.

The destabilizing effect of a nonuniform magnetic field with $dB/dz < 0$ is similar to the phenomenon of "magnetic buoyancy" analyzed by Parker[7] and by Weiss.[8] Magnetic buoyancy is attributed to an isolated tube of magnetic flux in thermal equilibrium with its nonmagnetic surroundings. The instability discussed here is due to the buoyancy of an arbitrary tube of flux within a smoothly varying magnetic field.

*Permanent address: Department of Mechanical and Aerospace Sciences, University of Rochester, Rochester, N.Y. 14627.

[1] W. A. Newcomb, Phys. Fluids 4, 391 (1961).
[2] C. P. Yu, Phys. Fluids 9, 412 (1966).
[3] K. Schwarzschild, Nachr. K. Ges. Wiss. Gött., p. 41 (1906); see also M. Schwarzschild, *Structure and Evolution of the Stars* (Princeton University, Princeton, NJ, 1958), p. 44.
[4] This was also shown by R. J. Tayler, J. Nucl. Energy C 3, 266 (1961).
[5] C. P. Yu, Phys. Fluids 8, 650 (1965).
[6] E. N. Parker, Astrophys. J. 145, 811 (1966).
[7] E. N. Parker, Astrophys. J. 121, 491 (1955).
[8] N. O. Weiss, Mon. Not. R. Astron. Soc. 128, 225 (1964).

SOLAR MAGNETO-ATMOSPHERIC WAVES. I. AN EXACT

SOLUTION FOR A HORIZONTAL MAGNETIC FIELD

Alan H. Nye and John H. Thomas*

Department of Mechanical and Aerospace Sciences
University of Rochester
Rochester, New York 14627

Running title: SOLAR MAGNETO-ATMOSPHERIC WAVES

*Also C. E. Kenneth Mees Observatory

ABSTRACT

The linearized theory of magneto-atmospheric waves (involving the combined restoring forces due to buoyancy, compressibility, and magnetic field) is developed for the case of a horizontal magnetic field. A general propagation equation is derived for adiabatic perturbations with arbitrary vertical distributions of the sound speed c, Alfvén velocity v_A, and local density scale height H. An exact analytical solution to the propagation equation is obtained for the case of an isothermal atmosphere permeated by a uniform horizontal magnetic field, without making the usual short-wavelength assumption. This solution is applied to an idealized model of the low-corona-chromosphere transition region for comparison with observations of flare-induced coronal waves. The results show that disturbances may propagate horizontally in the low corona in a wave guide formed by the sudden density increase into the chromosphere below and by the rapidly increasing Alfvén velocity with height in the corona. The group velocity of the guided wave modes is nearly independent of wavelength, so that a disturbance propagates as a compact wave packet.

23

I. INTRODUCTION

The theory of waves in a compressible, stratified, electrically-conducting atmosphere permeated by a magnetic field is of considerable importance in astrophysics, especially in solar physics where there is a wealth of detailed observations of such waves in the solar atmosphere. Following Yu (1965), we shall refer to waves which involve compressibility, buoyancy, and magnetic forces as magneto-atmospheric waves. Among the many solar phenomena that are seemingly attributable to magneto-atmospheric waves are the heating of the corona and of chromospheric plages, the five-minute oscillations in active regions, oscillations in sunspot umbrae and penumbrae, and flare-induced coronal disturbances.

The theory of magneto-atmospheric waves is complicated by the anisotropic nature of the medium; the gravitational field and the magnetic field each introduce preferred directions. Additionally, the disturbance is subjected to the combined restoring forces due to compressibility, buoyancy, and the magnetic field, so that pure wave modes (i.e., acoustic, Alfvén, and gravity) exist only as special cases. In general, magneto-atmospheric waves involve the effects of all three restoring forces. The problem is compounded by the fact that the basic parameters describing wave propagation in the solar atmosphere (the sound speed c, the Alfvén velocity v_A, and the local density scale height H) are, in general, functions of height, and therefore the

24

disturbance cannot be represented by plane waves propagating in the atmosphere.

Previously, the problem of magneto-atmospheric waves has been studied by either of two basic approaches, each yielding a dispersion relation based on constant values of the atmospheric parameters. The first approach has been to assume that the vertical extent of the disturbance is much less than the smallest scale height for variation of the atmospheric parameters. The parameters can then be taken as constant locally. McLellan and Winterberg (1968) studied an isothermal atmosphere permeated by a uniform magnetic field with arbitrary orientation. Then, assuming that the Alfvén velocity is constant locally (although it actually increases exponentially with height), they derived a local dispersion relation that is valid for short wavelengths (short compared to the density scale height). This local dispersion relation has been studied by several authors (Bel and Mein 1971; Michalitsanos 1973; Nakagawa, Priest, and Wellck 1973) to determine the effects of different propagation directions and magnetic field orientations.

The second basic approach has been to investigate an iso-thermal atmosphere permeated by a horizontal magnetic field that decreases exponentially with height such that the Alfvén velocity is constant, as are the sound speed and the density scale height. Yu (1965) derived the dispersion relation which in this case is valid for all wavelengths. He evaluated the three modes of propagation for various angles between the wave propagation vector

25

and the magnetic field. Chen and Lykoudis (1972) used the dispersion relation of Yu to study the five-minute oscillations in plage regions. Nye and Thomas (1974a) used Yu's dispersion relation in connection with a multi-layer model for running penumbral waves.

We consider only plane parallel atmospheres, with no horizontal variation, in order to permit Fourier decomposition in the horizontal directions as well as time. With variations in the z-direction only, the governing partial differential equations reduce to ordinary differential equations. There are only two magnetic field configurations consistent with static equilibrium and no horizontal variation. They are $\underline{B}$ = constant and $\underline{B} = (B_x(z), B_y(z), 0)$. We shall restrict our study to the case of a unidirectional horizontal magnetic field that may vary with height. We shall not follow either of the two basic approaches discussed above, however, due to the inherent limitations of each of them for solar applications. The length scale for magnetic field changes in the solar atmosphere is generally much greater than the density scale height, so that the assumption of constant Alfvén velocity is not justified. On the other hand, the length scale of observed disturbances in the solar atmosphere is not generally small compared to the density scale height. This is especially true in the photosphere where the density scale height may be smaller than 100 km, and hence smaller than the limit of observational resolution.

In section II we derive a general propagation equation for an arbitrary direction of propagation and arbitrary vertical variations of the atmospheric parameters. For the case of an isothermal atmosphere permeated by a uniform horizontal magnetic field, the Alfvén velocity increases exponentially with height. In section III we obtain an exact general solution of the propagation equation in this case. We compute eigenmodes for the case of a rigid lower boundary in section IV, and apply this to a specific solar wave phenomenon, the flare-induced coronal waves, in section V.

The analytical treatment in sections II and III also forms the basis of a following paper in which we deal with running penumbral waves.

II. BASIC EQUATIONS

The atmosphere is assumed to be a compressible, inviscid, perfectly conducting gas under a uniform acceleration of gravity g (=0.274 km sec^{-2}) in the negative z-direction. The undisturbed magnetic field is taken in the x-direction and may vary with height z; i.e., $\underline{B}_0 = (B_0(z),0,0)$. The undisturbed pressure, density, and temperature may all be functions of height z, and are denoted by $p_0(z)$, $\rho_0(z)$, and $T_0(z)$, respectively. We shall see that wave propagation in the basic atmosphere may be completely characterized by the vertical variation of the sound speed $c(z)$, the Alfvén velocity $v_A(z)$, and the local density

27

scale height $H(z)$, defined by

$$c^2 \equiv (\frac{\partial p_0}{\partial \rho_0})_s \quad , \quad v_A^2 \equiv \frac{B_0^2}{4\pi\rho_0} \quad , \quad \frac{1}{H} \equiv -\frac{1}{\rho_0}\frac{\partial \rho_0}{\partial z} \quad . \tag{1}$$

The unperturbed atmosphere is taken to be in static equilibrium:

$$\frac{d}{dz}(p_0 + \frac{B_0^2}{8\pi}) = -\rho_0 g \quad . \tag{2}$$

If the magnetic field is a function of height z, then it has a role in the basic equilibrium of the atmosphere. We consider only stable atmospheres, which requires that

$$\frac{dT_0}{dz} - (\frac{dT_0}{dz})_s > -\frac{1}{\rho_0 R}\frac{d}{dz}(\frac{B_0^2}{8\pi}) \quad ,$$

where $(dT_0/dz)_s$ is the adiabatic temperature gradient and R is the gas constant (see Thomas and Nye (1975) for a recent discussion).

Consider small adiabatic perturbations of the equilibrium atmosphere, letting p, ρ, $\underline{u}$, and $\underline{B}$ denote the perturbations in pressure, density, velocity, and magnetic field, respectively. Then, the basic linearized equations of continuity, momentum, energy, and induction are

$$\frac{\partial \rho}{\partial t} + \nabla \cdot (\rho_0 \underline{u}) = 0 \quad , \tag{3}$$

$$\rho_0 \frac{\partial \underline{u}}{\partial t} + \nabla p - \rho \underline{g} - \frac{1}{4\pi}\left\{(\nabla \times \underline{B}_0) \times \underline{B} + (\nabla \times \underline{B}) \times \underline{B}_0\right\} = 0, \tag{4}$$

$$\frac{\partial p}{\partial t} + \underline{u} \cdot \nabla p_0 = c^2 [\frac{\partial \rho}{\partial t} + \underline{u} \cdot \nabla \rho_0] \quad , \tag{5}$$

28

$$\frac{\partial \underline{B}}{\partial t} - \nabla \times (\underline{u} \times \underline{B}_0) = 0 \quad . \tag{6}$$

After taking the time derivative of the momentum equation (4), we may eliminate the perturbation quantities p, ρ, and $\underline{B}$ by using equations (3), (5), and (6). This leaves a single vector equation for the velocity perturbation $\underline{u} = (u,v,w)$:

$$\rho_0 \frac{\partial^2 \underline{u}}{\partial t^2} + \nabla \left\{ \rho_0 w [g + \frac{1}{8\pi\rho_0} \frac{dB_0^2}{dz}] - c^2 \rho_0 \nabla \cdot \underline{u} \right\} +$$

$$+ \left\{ (\underline{u} \cdot \nabla)\rho_0 + \rho_0 \nabla \cdot \underline{u} \right\} \underline{g} - \frac{1}{4\pi} \left\{ (\nabla \times \underline{B}_0) \times [\nabla \times (\underline{u} \times \underline{B}_0)] - \right.$$

$$\left. - \underline{B}_0 \times (\nabla \times [\nabla \times (\underline{u} \times \underline{B}_0)]) \right\} = 0 \quad . \tag{7}$$

Next, we assume that the perturbation velocity has the form $\underline{u} = \underline{\hat{u}} \exp i(\underline{k} \cdot \underline{r} - \omega t)$, with $\underline{\hat{u}} = \underline{\hat{u}}(z) = (\hat{u}(z), \hat{v}(z), \hat{w}(z))$ and $\underline{k} \cdot \underline{r} = k_x x + k_y y$. Then, using the definition of v_A^2, the three components of the momentum equation (7) become

$$(\omega^2 - c^2 k_x^2)\hat{u} - c^2 k_x k_y \hat{v} - ik_x(g - c^2 \frac{d}{dz})\hat{w} = 0 \quad , \tag{8}$$

$$- c^2 k_x k_y \hat{u} + [\omega^2 - c^2 k_y^2 - v_A^2(k_x^2 + k_y^2)]\hat{v} - ik_y[g -$$

$$- (c^2 + v_A^2)\frac{d}{dz}]\hat{w} = 0 \quad , \tag{9}$$

and

$$ik_x \left\{ \frac{dc^2}{dz} - \frac{c^2}{H} + g + c^2\frac{d}{dz} \right\} \hat{u} + ik_y \left\{ \frac{d}{dz}(c^2 + v_A^2) - \right.$$

$$\left. - \frac{(c^2 + v_A^2)}{H} + g + (c^2 + v_A^2)\frac{d}{dz} \right\} \hat{v} + (c^2 + v_A^2)\frac{d^2\hat{w}}{dz^2} +$$

$$+ \left\{ \frac{d}{dz}(c^2 + v_A^2) - \frac{(c^2 + v_A^2)}{H} \right\} \frac{d\hat{w}}{dz} + (\omega^2 - v_A^2 k_x^2)\hat{w} = 0 \quad . \tag{10}$$

29

These are the linearized perturbation equations. They give important information about particle motions for various modes of propagation in the atmosphere.

The horizontal components of the perturbation velocity can be eliminated from the system of equations (8) - (10) to yield a single equation for the vertical velocity $\hat{w}$. The resulting equation is

$$\frac{d^2\hat{w}}{dz^2} + A(z)\,\frac{d\hat{w}}{dz} + B(z)\,\hat{w} = 0 \quad , \tag{11}$$

where the coefficients $A(z)$ and $B(z)$ are given by

$$A(z) = -\frac{1}{H} + \frac{\omega^4}{DE}(\omega^2 - v_A^2 k_x^2)^2\,\frac{dc^2}{dz} + \frac{1}{D}[-\omega^4 +$$

$$+ (\omega^2 - c^2 k_x^2)(\omega^2 - v_A^2 k_x^2)(1 + \frac{\omega^4}{E})]\frac{dv_A^2}{dz} \tag{12}$$

and

$$B(z) = \frac{1}{D}\Big\{\omega^6 - [(c^2 + v_A^2)(k_x^2 + k_y^2) + v_A^2 k_x^2]\omega^4 + [v_A^2 k_x^2(k_x^2 + k_y^2)(2c^2 + v_A^2) -$$

$$- g(k_x^2 + k_y^2)(g - \frac{c^2}{H}) + \frac{g}{H}v_A^2 k_y^2]\omega^2 - v_A^2 k_x^2(k_x^2 + k_y^2)[c^2 v_A^2 k_x^2 -$$

$$- g(g - \frac{c^2}{H})] - \frac{g}{E}(\omega^2 - v_A^2 k_x^2)^2\omega^2(k_x^2 + k_y^2)\frac{dc^2}{dz} - \frac{\omega^6}{E}k_y^2 g\frac{dv_A^2}{dz}\Big\} \quad . \tag{13}$$

Here, D and E are given by

$$D = (\omega^2 - v_A^2 k_x^2)[\omega^2(c^2 + v_A^2) - c^2 v_A^2 k_x^2] \tag{14}$$

and

$$E = \omega^4 - (k_x^2 + k_y^2)[\omega^2(c^2 + v_A^2) - c^2 v_A^2 k_x^2] \quad . \tag{15}$$

30

Equation (11) is a general equation for the vertical component of velocity for a perturbation propagating in an arbitrary direction, in an atmosphere with a horizontal magnetic field and arbitrary vertical distributions of c^2, v_A^2, and H. This propagation equation has been given previously (Nye and Thomas 1974a) in the case $k_y = 0$.

III. ISOTHERMAL ATMOSPHERE WITH A UNIFORM
HORIZONTAL MAGNETIC FIELD

Now consider the case where the undisturbed temperature and magnetic field are constant with height. Since the magnetic field is uniform, it has no effect on the hydrostatic equilibrium of the atmosphere, and the equilibrium pressure and density both decrease exponentially with height. The sound speed and the density scale height are both constant, with values determined by the temperature of the atmosphere. The Alfvén velocity increases exponentially with height due to the decreasing density. The sound speed, density scale height, density, and Alfvén velocity are given by

$$c = (\gamma R T_0)^{\frac{1}{2}} = \text{const.} \quad , \tag{16}$$

$$H = \frac{RT_0}{g} = \text{const.} \quad , \tag{17}$$

$$\rho_0(z) = \rho_{00} e^{-z/H} \quad , \tag{18}$$

and

31

$$v_A(z) = v_0 e^{z/2H} \quad , \tag{19}$$

where ρ_{00} and v_0 are the values of the undisturbed density and Alfvén velocity at $z = 0$.

The nondimensional parameter $\beta^2 \equiv v_0^2/c^2$ is introduced as a measure of the relative importance of the restoring forces due to the magnetic field and to compressibility at the point $z = 0$. For values of $\beta^2 < 1$, there is a region of the atmosphere above $z = 0$ where compressibility has more importance as a restoring force than does the magnetic force, but in any case the magnetic field always becomes dominant as z becomes large.

In the remainder of this paper we shall consider only waves whose horizontal component of propagation is parallel to the magnetic field ($k_y = 0$). Using (16) - (19), we may write (11) as

$$[c^2\omega^2 + (\omega^2 - c^2 k_x^2) v_0^2 e^{z/H}] \frac{d^2\hat{w}}{dz^2} - \frac{c^2\omega^2}{H} \frac{d\hat{w}}{dz} +$$

$$+ [(\omega^2 - c^2 k_x^2)(\omega^2 - v_0^2 e^{z/H} k_x^2) - g(g - \frac{c^2}{H}) k_x^2]\hat{w} = 0 \quad . \tag{20}$$

We define the nondimensional frequency Ω and the non-dimensional horizontal wavenumber K by

$$\Omega \equiv \frac{H\omega}{c} \quad , \qquad K \equiv Hk_x \quad . \tag{21}$$

By transforming the dependent and independent variables according to

$$W = \hat{w} e^{zK/H} \quad , \qquad x = \frac{\Omega^2}{\beta^2(K^2 - \Omega^2)} e^{-z/H} \quad ,$$

32

we may put equation (20) in the dimensionless form

$$x(1-x)\frac{d^2W}{dx^2} + [C-(A+B+1)x]\frac{dW}{dx} - ABW = 0 \ , \tag{23}$$

with

$$A + B = C = 2K + 1 \ , \qquad AB = \Omega^2 + K + (\frac{\gamma-1}{\gamma^2})\frac{K^2}{\Omega^2} \ . \tag{24}$$

Equation (23) is the standard form of the hypergeometric differential equation.[1] The solutions of this equation may be expressed in terms of hypergeometric functions, given for $|x| < 1$ by

$$F(A,B;C;x) = \frac{\Gamma(C)}{\Gamma(A)\Gamma(B)} \sum_{n=0}^{\infty} \frac{\Gamma(A+n)\Gamma(B+n)}{\Gamma(C+n)} \frac{x^n}{n!} \ . \tag{25}$$

The general solution of equation (23) may be written, for $|x| < 1$, in terms of the original variables z and $\hat{w}(z)$ as

$$\hat{w}(z) = D_1 e^{-zK/H} F(A,B;C;\frac{\Omega^2}{\beta^2(K^2-\Omega^2)} e^{-z/H}) +$$

$$+ D_2 e^{zK/H} [\frac{\beta^2(K^2-\Omega^2)}{\Omega^2}]^{2K} F(A-C+1,B-C+1;2-C;\frac{\Omega^2}{\beta^2(K^2-\Omega^2)} e^{-z/H}) , \tag{26}$$

where D_1 and D_2 are arbitrary constants.

IV. EIGENMODES FOR A RIGID LOWER BOUNDARY

We now examine modes of propagation in the relatively simple

_____

[1]The hypergeometric nature of the wave equation in this case was noted by us earlier (Nye and Thomas 1974b), and also independently by Adam (1974).

33

case of an isothermal atmosphere with a uniform horizontal magnetic field, bounded from below by a rigid wall at $z = 0$. The general solution (26) is subject to boundary conditions at $z = 0$ $(x = \Omega^2/\beta^2(K^2-\Omega^2))$ and at $z = \infty$ $(x = 0)$.

As a condition at $z = \infty$, we require that the total energy of the perturbation be integrable over $0 \leq z < \infty$. The magnetic energy of the perturbation is proportional to the square of the velocity. Since

$$\lim_{x \to 0} F(\alpha, \beta; \gamma; x) = 1 \quad , \tag{27}$$

we see from (26) that we must take $D_2 = 0$.

The second boundary condition is that the vertical velocity vanish at the rigid wall, i.e., $\hat{w} = 0$ at $z = 0$, i.e., at $x = \Omega^2/\beta^2(K^2-\Omega^2)$. Provided

$$\left| \frac{\Omega^2}{\beta^2(K^2-\Omega^2)} \right| < 1 \quad , \tag{28}$$

we may apply this condition directly to (26) with $D_2 = 0$ to obtain the dispersion relation

$$F(A, B; C; \frac{\Omega^2}{\beta^2(K^2-\Omega^2)}) = 0 \quad , \tag{29}$$

If, however, (28) is not satisfied, then other representations of the general solution (26), valid for $|x| \geq 1$ must be used in order to apply the boundary condition at $z = 0$. For

$$\frac{\Omega^2}{\beta^2(K^2-\Omega^2)} \geq 1 \quad , \tag{30}$$

34

the interval $0 \leq x \leq \Omega^2/\beta^2(K^2-\Omega^2)$ contains the regular singular point at $x = 1$, and no solution that satisfies the boundary conditions and is also regular at $x = 1$ is to be expected. For the range

$$\frac{\Omega^2}{\beta^2(K^2-\Omega^2)} \leq -1 \quad , \qquad (31)$$

we may use analytic continuation to extend the general solution (26). The analytic continuation of (26) with $D_2 = 0$, valid for $x \leq -1$, is given by

$$\hat{w}(z) = D_1 e^{-zK/H} \left\{ \frac{\Gamma(C)\Gamma(B-A)}{[\Gamma(B)]^2} \left[\frac{\beta^2(\Omega^2-K^2)}{\Omega^2} \right]^A e^{zA/H} \times \right.$$

$$\times \; F(A,1-B;1-B+A;\frac{\beta^2(K^2-\Omega^2)}{\Omega^2} e^{z/H}) + \frac{\Gamma(C)\Gamma(A-B)}{[\Gamma(A)]^2} \times$$

$$\times \; \left[\frac{\beta^2(\Omega^2-K^2)}{\Omega^2} \right]^B e^{zB/H} F(B,1-A;1-A+B;\frac{\beta^2(K^2-\Omega^2)}{\Omega^2} e^{z/H}) \left. \right\} . \qquad (32)$$

Thus, for the range of parameters (31), the dispersion relation is given by

$$\frac{\Gamma(B-A)}{[\Gamma(B)]^2} \left[\frac{\beta^2(\Omega^2-K^2)}{\Omega^2} \right]^A F(A,1-B;1-B+A;\frac{\beta^2(K^2-\Omega^2)}{\Omega^2}) +$$

$$+ \; \frac{\Gamma(A-B)}{[\Gamma(A)]^2} \left[\frac{\beta^2(\Omega^2-K^2)}{\Omega^2} \right]^B F(B,1-A;1-A+B;\frac{\beta^2(K^2-\Omega^2)}{\Omega^2}) = 0 . \qquad (33)$$

The dispersion relation (equation (29) or (33)) has been evaluated for various values of the nondimensional parameter β^2. Examples are plotted in figures 1 and 2 (also see figure 4). The curves in these figures represent well-defined eigenmodes of wave propagation in the atmosphere. These curves represent

trapped waves propagating horizontally in the waveguide formed by the solid boundary below and the exponentially increasing Alfvén velocity above.

There are several ways of interpreting the effect of changing β^2 on the dispersion relation. First, different values of β^2 can be taken to represent the same magnetic field strength and the same density at $z = 0$, but different atmospheric temperatures. A second interpretation is that different values of β^2 represent the same magnetic field strength and the same temperature, but different densities. This is equivalent to placing the solid lower boundary at successively higher levels in the atmosphere corresponding to larger values of β^2. At each higher level the magnetic restoring force becomes more important due to the decreased density, while the compressible restoring force remains the same.

The third interpretation is to consider changes in β^2 to be due to changes in the magnetic field strength, with fixed values of temperature and density. Since the sound speed and the density scale height then do not change, the scales for the frequency and horizontal wavenumber are the same in each case and the dispersion diagrams can be compared directly. From figures 1 and 2 it can be seen that increasing the magnetic field strength (increasing β^2) increases the cutoff frequency. As β^2 increases, the slope of the dispersion curves, and hence the group velocity, also increases.

Lowering the value of γ to represent crudely the effect of

radiative transfer has little effect on the nondimensional

dispersion diagrams. However, the frequency scaling depends

on γ as $\omega \sim (\gamma)^{\frac{1}{2}}\Omega$, while the wavenumber scaling is independent

of γ. Therefore, for lower γ (lower sound speed) the wave

oscillates less rapidly and the phase and group velocities are

correspondingly lower.

The vertical velocity of the disturbance (equation (26) or

(32)) can be calculated as a function of height for any point

on a dispersion curve. Figure 3 compares the lowest mode of

oscillation for the same horizontal wavenumber but different

values of β^2 (i.e., different magnetic field strengths), and

shows that for increasing magnetic field strength, the wave

oscillates more rapidly and is trapped at lower levels in the

atmosphere. We now discuss the eigenmodes given by the dispersion

relation (29) or (33) in relation to an observed solar

oscillation.

V.   APPLICATION TO FLARE-INDUCED CORONAL WAVES

On September 20, 1963, Moreton and Ramsey (Moreton 1965)

observed a chromospheric disturbance, apparently caused by the

flash phase of a flare, propagate at a nearly constant velocity

of 750 km s^{-1} for several hundred thousand kilometers across

the solar disk. Many other flare-induced disturbances have

been reported (Moreton 1960, Athay and Moreton 1961, Dodson and

Hedeman 1968) and the propagation velocity is usually on the order

37

of 1000 km s^{-1}. Dodson and Hedeman (1968) report that the width of the disturbance created by the proton flare of August 28, 1966 was greater than 100,000 km.

These disturbances could not have been propagating solely in the chromosphere, since in the chromosphere the sound speed is only of the order of 20 km s^{-1} and the Alfvén velocity is only of the order of 50 km s^{-1}. Thus a purely chromospheric disturbance would have created a shock wave and been rapidly dissipated. In the corona, however, both the Alfvén velocity and the sound speed are an order of magnitude higher than in the chromosphere due to the increased temperature and decreased density. It has been proposed (Meyer 1968; Uchida 1968, 1970, 1974; Uchida et al. 1973) that the disturbance is a magneto-hydrodynamic wave propagating in the low corona and that the motion of this wave at the corona-chromosphere transition region is what is actually observed. There is, however, no general agreement as to the wavelength of the disturbance or even whether the observed disturbance is a single wave or a wave packet.

Meyer (1968) studied the propagation of the magneto-acoustic fast mode in an isothermal corona permeated by a uniform vertical magnetic field, with a rigid lower boundary representing the chromosphere-corona transition region. He found eigenmodes with nearly constant horizontal group velocity. Equating the group velocity to the observed propagation velocity, Meyer found that for a horizontal wavelength on the order of 100,000 km, the coronal magnetic field must be approximately 6 gauss, a

38

reasonable average value.

Uchida, in a series of papers (Uchida 1968, 1970, 1974; Uchida et. al. 1973), studied the propagation of short wavelength (∼5000 km) disturbances in various realistic coronal models. Using a ray-tracing technique, he obtained horizontal and vertical refractions in close agreement with the observed waves.

Although the magnetic field structure of the corona is quite complicated, the field changes fairly slowly and there are probably regions of nearly uniform field with almost any orientation. We study the case of a uniform horizontal field in connection with the coronal wave problem only as a means of understanding the mechanism of wave propagation for waves of arbitrary wavelength. Our model supplements Meyer's (1968) work by considering the case of a uniform horizontal magnetic field, and by including effects of gravity and stratification. As in Meyer's model, we use the rigid lower boundary to represent upward reflection from the chromosphere-corona transition layer.

We have evaluated our solution for a temperature of 1.6×10^6 °K and $\beta^2 = 10$, which is fairly typical of the base of the corona. These values correspond to a sound speed of 180 km s^{-1} and a density scale height of approximately 71,000 km. Figure 4 shows the dimensional dispersion relation for these parameters. We see that the dispersion curves are nearly straight, which means that these modes have very little dispersion and will propagate for great distances with little change in character.

39

The first three modes have been calculated for a wavelength of 75,000 km in figure 5. The first mode has nearly zero vertical velocity above two scale heights and is therefore trapped in the low corona.

The phase velocity and group velocity of the first mode have been plotted as a function of horizontal wavenumber in figure 6. For any wavelength of 100,000 km or less, the group velocity is nearly constant at about 610 km s^{-1}. Since the energy of a disturbance propagates at the group velocity, it is not important which specific wavelength, or spectrum of wavelengths, receives energy from the flare. The energy at all wavelengths will propagate together as a wave packet near the lower coronal boundary.

The present model is not proposed as a realistic model of the solar corona, although it may be fairly accurate over certain regions. No attempt has been made to include the effects of horizontal variations. The value of the model is that a mechanism for wave propagation can be studied for arbitrary wavelengths. These results close the gap between the short wavelength ray-tracing theory and the long wavelength, vertical field case. We show that the question of wavelength is not particularly important since the group velocity of the trapped modes is essentially independent of wavelength. For the relatively large value of β^2 (=10), the wave modes are basically the magneto-acoustic fast modes (studied by Meyer and by Uchida) modified by gravity. For an inclined magnetic field, there must

40

also be trapped modes of propagation involving a coupling of the present modes and the type of mode studied by Meyer for a vertical field. The present results, taken with those of Meyer and the work of Uchida, present a consistent picture of flare-induced coronal waves as guided magneto-atmospheric waves.

ACKNOWLEDGEMENTS

REFERENCES

Adam, J. A. 1974, Ph.D. Thesis, University of London.

Athay, R. G., and Moreton, G. E. 1961, Astrophys. J. 133, 935.

Bel, N., and Mein, P. 1971, Astron. and Astrophys. 11, 234.

Chen, J. C., and Lykoudis, P. S. 1972, Solar Phys. 25, 380.

Dodson, H. W., and Hedeman, E. R. 1968, Solar Phys. 4, 229.

McLellan, A., and Winterberg, F. 1968, Solar Phys. 4, 401.

Meyer, F. 1968, in Kiepenheuer (ed.), "Structure and Development
    of Solar Active Regions", I.A.U. Symp. 35, 485.

Michalitsanos, A. G. 1973, Solar Phys. 30, 47.

Moreton, G. E. 1960, Astron. J. 65, 494.

Moreton, G. E. 1965, in "Stellar and Solar Magnetic Fields",
    I.A.U. Symp. 22, 371.

Nakagawa, Y., Priest, E. R., and Wellck, R. E. 1973, Astrophys.
    J. 184, 931.

Nye, A. H., and Thomas, J. H. 1974a, Solar Phys. 38, 399.

Nye, A. H., and Thomas, J. H. 1974b, Bull. Am. Phys. Soc. 19,
    1148.

Thomas, J. H., and Nye, A. H. 1975, Phys. Fluids 18, 490.

Uchida, Y. 1968, Solar Phys. 4, 30.

Uchida, Y. 1970, Publ. Astr. Soc. Japan 22, 341.

Uchida, Y. 1974, Solar Phys. 39, 431.

Uchida, Y., Altschuler, M. D., and Newkirk, G., Jr. 1973, Solar
    Phys. 28, 495.

Yu, C. P. 1965, Phys. Fluids 8, 650.

FIGURE CAPTIONS

Fig. 1   Dispersion diagrams (nondimensional frequency versus
          nondimensional horizontal wavenumber) for an isothermal
          atmosphere with a uniform horizontal magnetic field
          and a solid lower boundary, with $\gamma = 5/3$, $\beta^2 = 10^{-5}$,
          and $\beta^2 = 10^{-4}$. The curves represent eigenmodes and the
          crosses indicate the computed points. This figure
          should not be confused with a diagnostic diagram for an
          atmosphere with constant parameters (e.g., Yu 1965).

Fig. 2   Same as Fig. 1, but with $\beta^2 = 0.5$.

Fig. 3   Direct comparison of the first mode of oscillation
          of the atmosphere for the same nondimensional horizontal
          wavenumber ($K = 0.25$) but for two values of β^2
          ($\beta^2 = 10^{-3}$, $\beta^2 = 10^{-1}$).

Fig. 4   Dimensional dispersion diagram for $\beta^2 = 10$, $\gamma = 5/3$,
          and $T = 1.6 \times 10^{6}$°K. The curves represent eigenmodes
          of the corona which are trapped by the increasing
          Alfvén velocity with height.

Fig. 5   First three modes of oscillation of the model corona
          for $\beta^2 = 10$, $\gamma = 5/3$. The vertical velocities have
          been normalized to maximum value unity.

Fig. 6   Phase velocity v_p and group velocity v_g of the first
          mode of coronal oscillation plotted as a function of
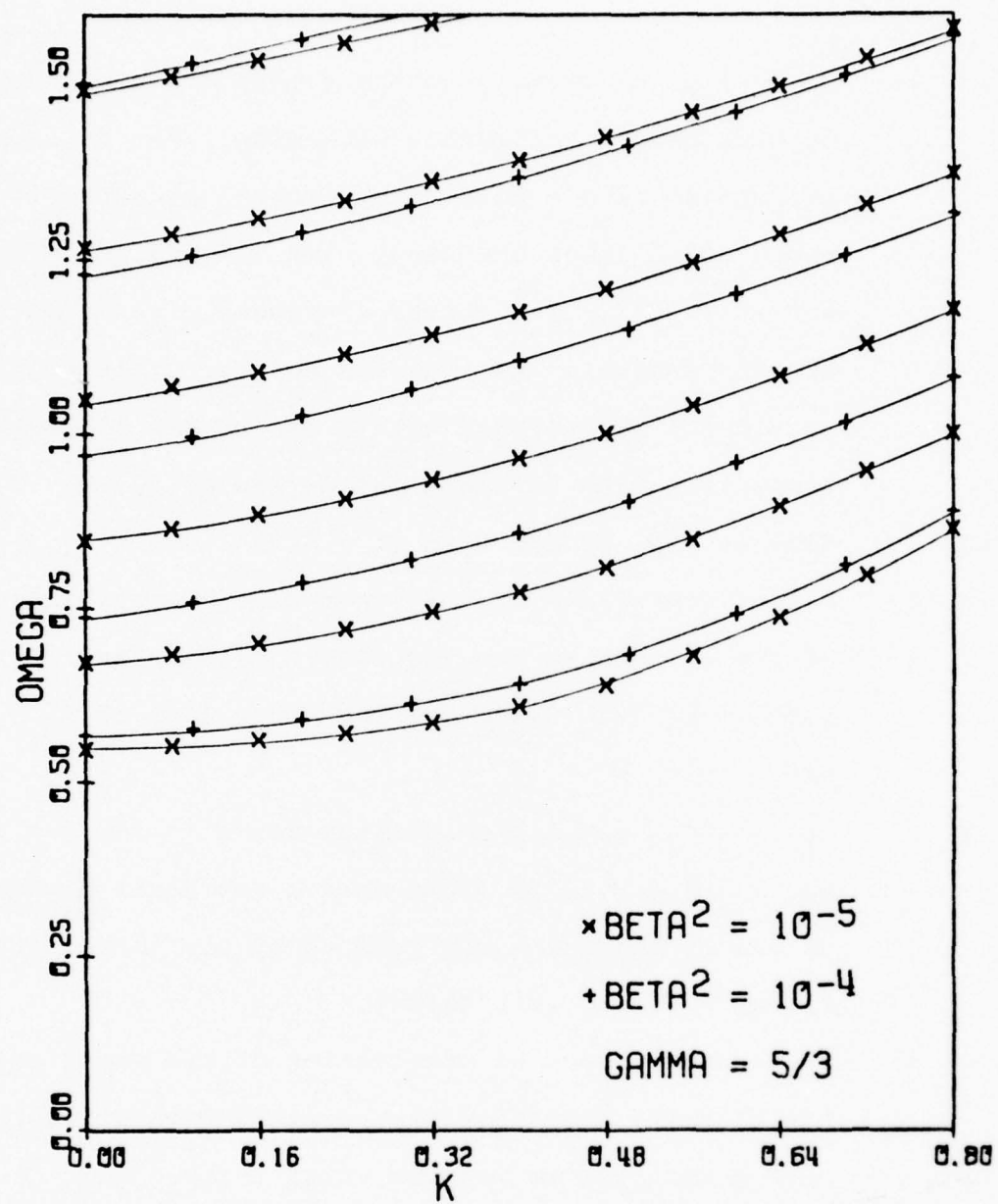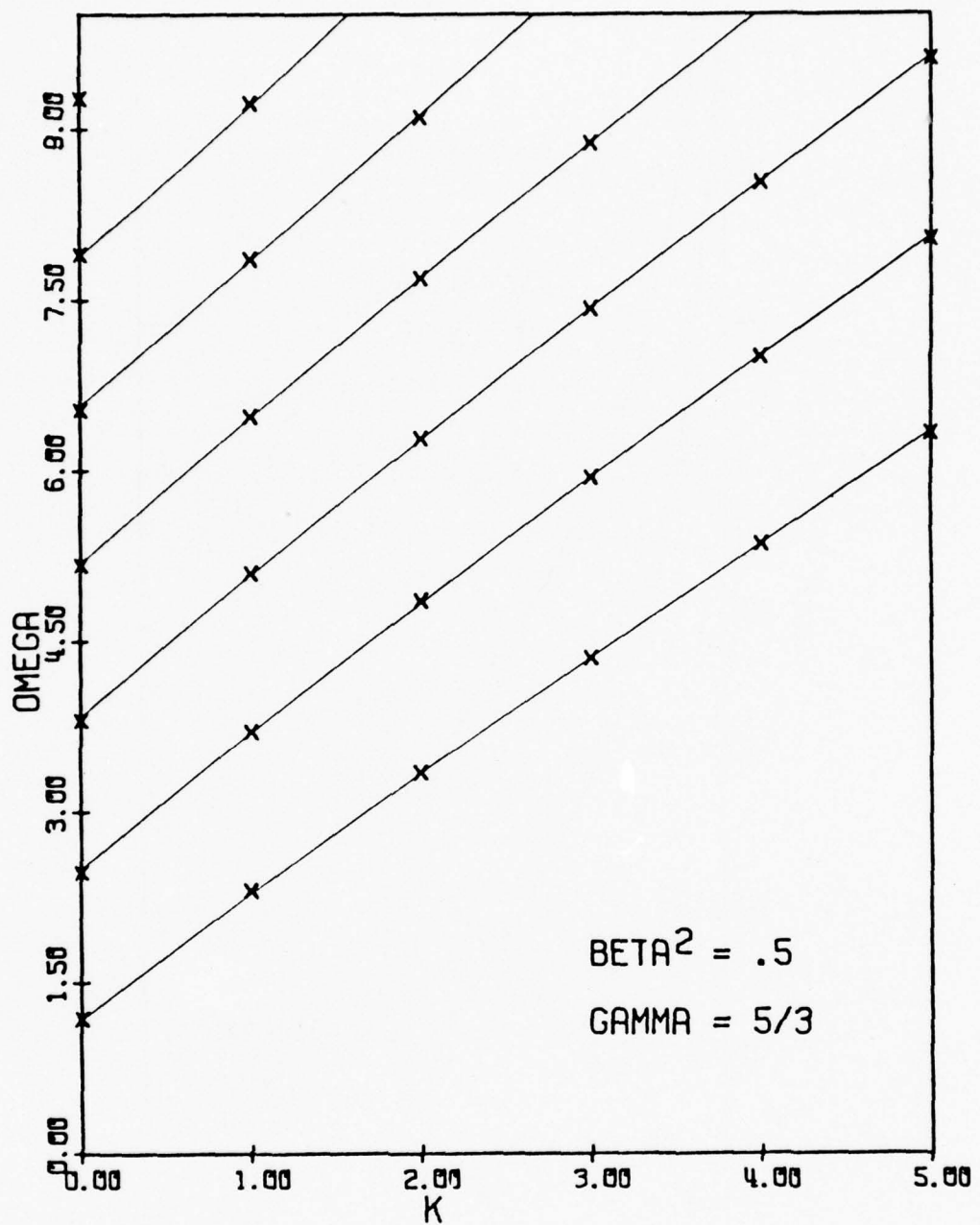   horizontal wavenumber.
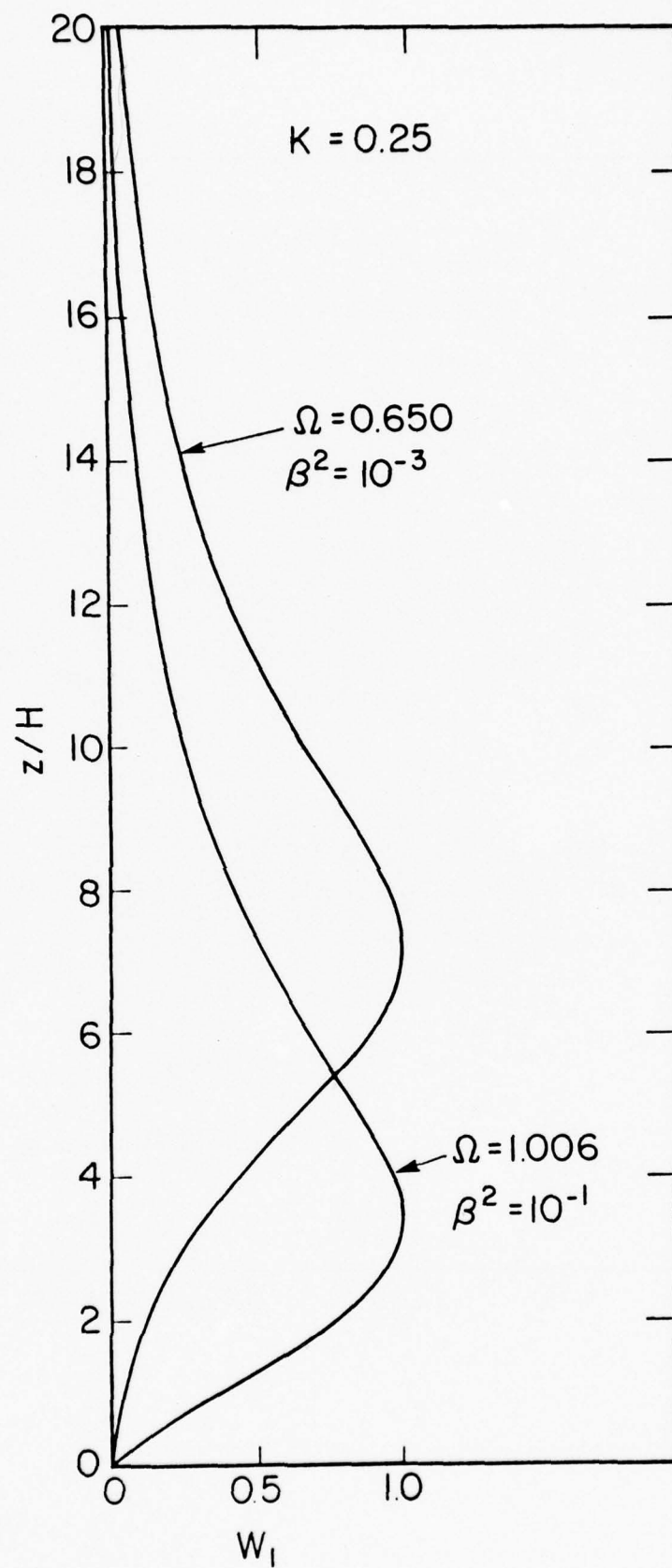
43

Fig. 1

44

Fig. 2

45

Fig. 3

46

Fig. 4

47

$K = 3.5$

$\beta^2 = 10$

$\gamma = 5/3$

$\Omega_1 = 17.7$

$\Omega_2 = 23.7$

$\Omega_3 = 29.3$

w_1

w_2

w_3

z/H

4.0 3.6 3.2 2.8 2.4 2.0 1.6 1.2 0.8 0.4 0

0.5 1.0

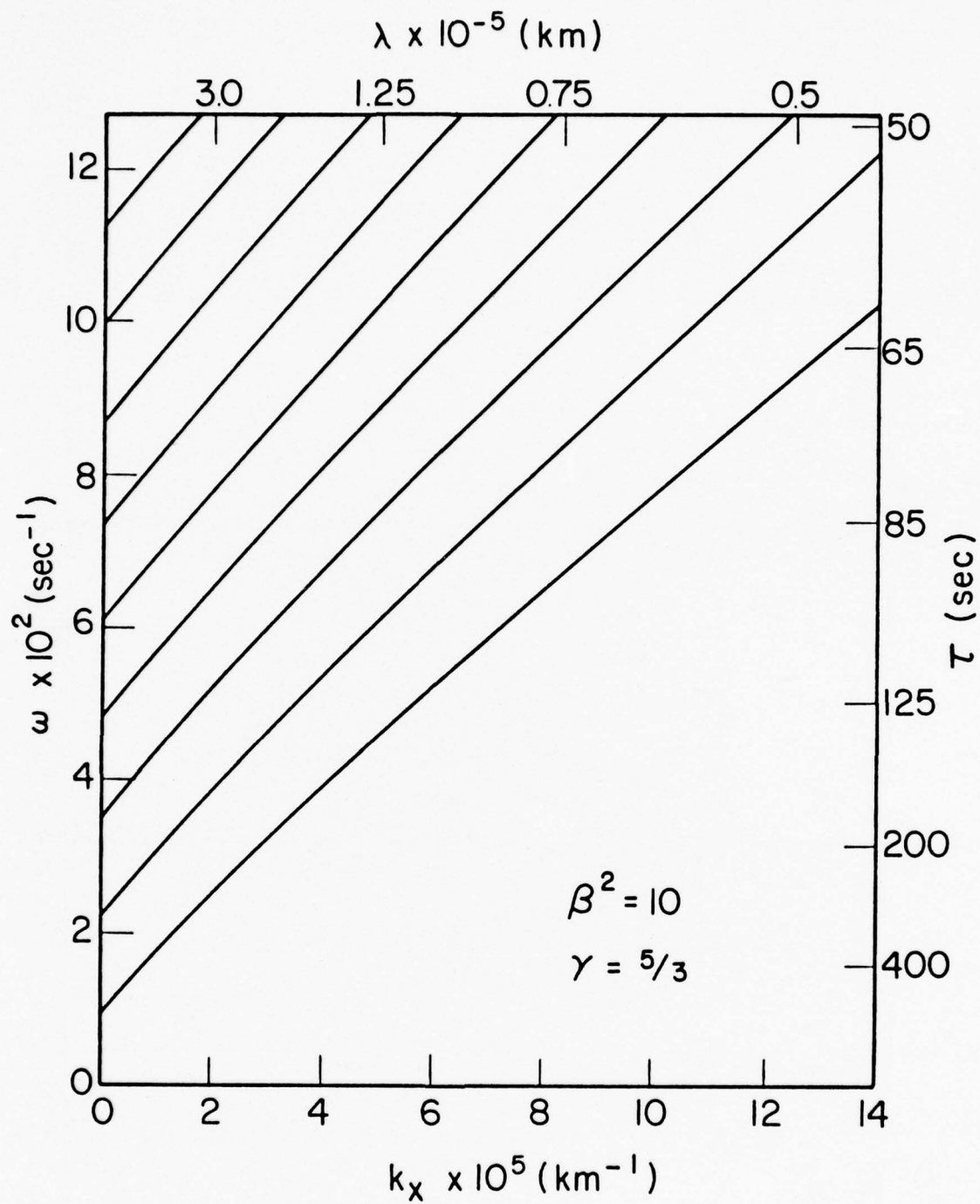0.0 0.5 1.0

−0.5 0.0 0.5 1.0

−0.5 0.0 0.5 1.0

Fig. 5

48
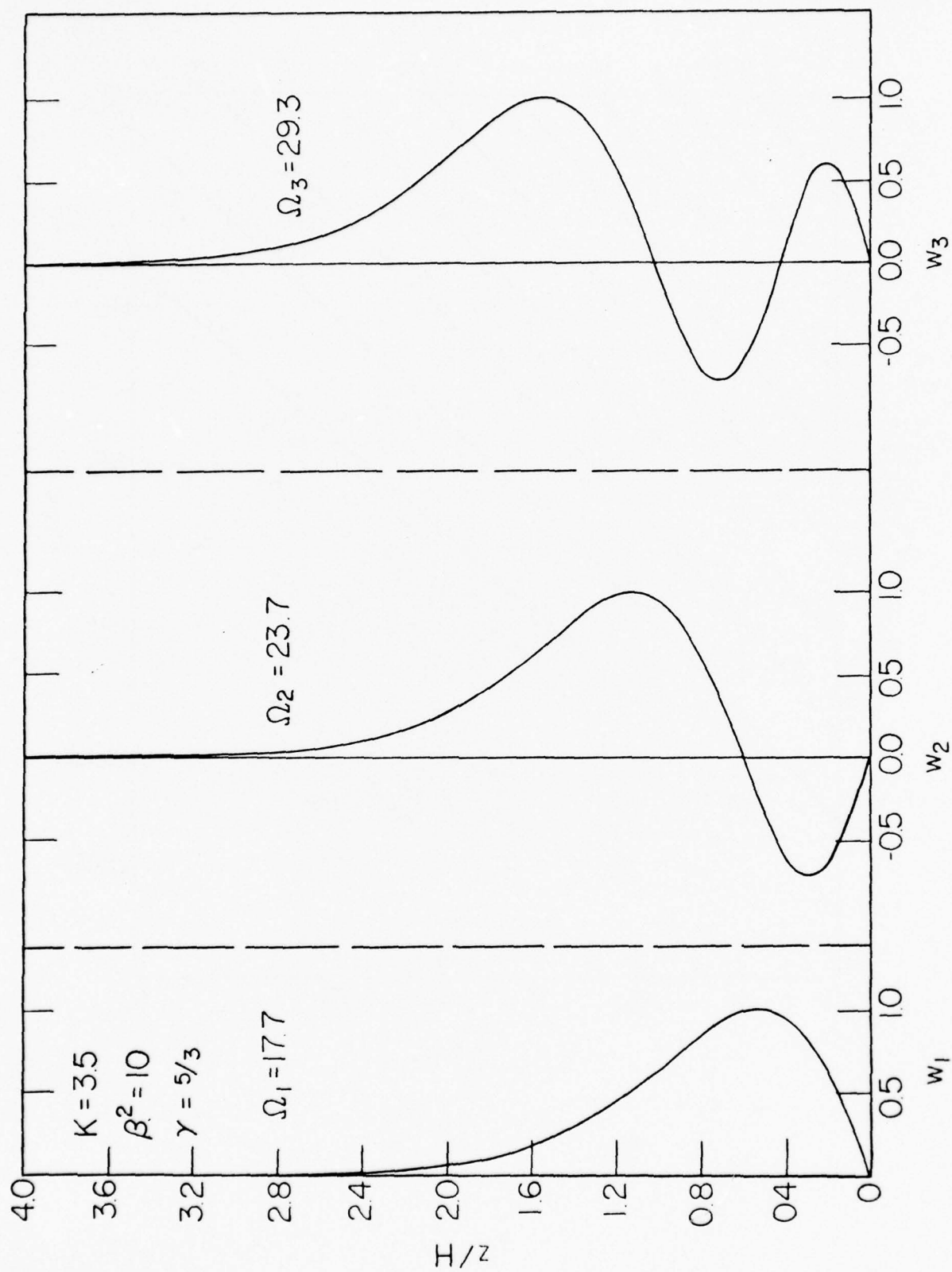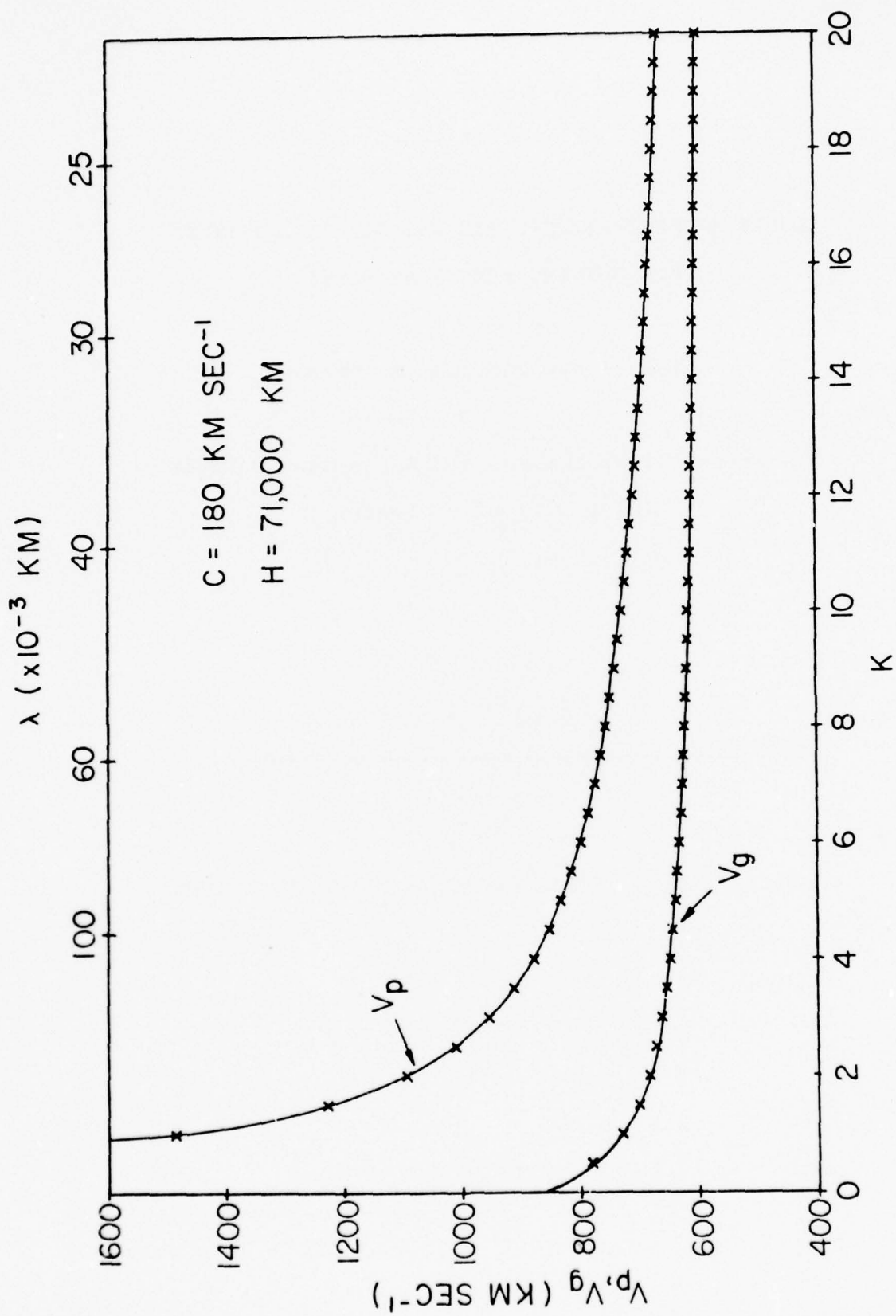
Fig. 6

49

SOLAR MAGNETO-ATMOSPHERIC WAVES. II. A MODEL

FOR RUNNING PENUMBRAL WAVES

Alan H. Nye and John H. Thomas*

Department of Mechanical and Aerospace Sciences

University of Rochester

Rochester, New York 14627

Running title: SOLAR MAGNETO-ATMOSPHERIC WAVES

*also C. E. Kenneth Mees Observatory

ABSTRACT

A simple two-layer model of a sunspot penumbra is used
to study the mode of running penumbral waves. Exact solutions
of the linearized wave equation, not limited to the small-
wavelength approximation, are employed in each layer. The
lowest "plus" eigenmode of magneto-atmospheric waves in the
model penumbra is in good agreement with observations of
running penumbral waves. The results indicate that running
penumbral waves should be observable in a photospheric spectral
line.

I. INTRODUCTION

In Paper I of this series (Nye and Thomas 1975) we presented an exact analytical solution for magneto-atmospheric waves in the case of an isothermal atmosphere with a uniform horizontal magnetic field. In the present paper we apply this solution to a simple two-layer model penumbra in order to study the mode of running penumbral waves.

Running penumbral waves (Zirin and Stein 1972; Giovanelli 1972, 1974; Moore and Tang 1975) are good examples of magneto-atmospheric waves. These waves propagate radially outward across sunspot penumbrae, with predominantly vertical motions in $H\alpha$. The observed range of frequency and propagation speed is fairly well established (see discussion in section IV).

Moore (1973) has concluded that the source of excitation of the penumbral waves is overstable convection in the low umbra. In an earlier paper (Nye and Thomas 1974 (NT)) we studied the mode of propagation of penumbral waves on the basis of a piece-wise linear model of the vertical structure of a typical sunspot penumbra. We found the penumbral waves to be magneto-atmospheric waves (of the "plus" type) that are vertically trapped at photo-spheric levels. This trapping is primarily due to the increasing sound speed with depth into the convection zone and the increasing Alfvén velocity with height into the chromosphere.

Here we extend our earlier work by computing actual eigen-modes of propagation for a somewhat simpler model penumbra, which

52

nevertheless retains the essential features. The properties of the lowest mode of propagation of the model penumbra turn out to be in good agreement with observations, and give some useful clues for further observation of running penumbral waves.

II. THE TWO-LAYER PENUMBRAL MODEL

The entire penumbral model consists of a compressible, inviscid, perfectly-conducting, stratified perfect gas subject to a constant acceleration of gravity g (= 0.274 km s^{-2}) in the negative z-direction. The upper layer is isothermal and is permeated by a uniform horizontal magnetic field, which yields an Alfvén velocity that increases exponentially with height due to the decreasing density. An exact solution of the linearized propagation equation for this case was given in Paper I.

This upper layer is a suitable model of the penumbral photo-sphere and chromosphere, where observed penumbral magnetic fields are very nearly horizontal (Nishi and Makita 1973) and decrease slowly with height (Bray and Loughhead 1964). The scale height for variation of the magnetic field is very large compared to the density scale height, so the assumption of a uniform horizontal magnetic field is reasonable. Our earlier calculations (NT) showed that running penumbral waves are trapped at photospheric levels, so that the increasing sound speed in the upper chromosphere has little effect on the trapping. Taking the upper layer to be iso-thermal is therefore also a reasonable assumption.

53

The vertical distributions of the sound speed and Alfvén velocity for the two-layer model penumbra are shown in Figure 1. Subscripts 1 and 2 denote quantities in the upper and lower layers, respectively, and the subscript 0 refers to quantities evaluated at $z = 0$. The sound speed, density scale height, and Alfvén velocity in the upper layer are given by

$$c_1^2 = \gamma_1 R T_1 = \text{const.} \,, \tag{1}$$

$$H_1 = \frac{c_1^2}{\gamma_1 g} = \text{const.} \,, \tag{2}$$

and

$$v_A^2(z) = v_0^2 e^{z/H_1} \,. \tag{3}$$

The lower layer of the penumbral model (layer 2, figure 1) is adiabatic with no magnetic field. The temperature decreases with height (increases with depth) at the adiabatic lapse rate, $(dT/dz)_s = -g/c_p$, and thus this layer is neutrally stable. The actual temperature distribution in the convection zone below a penumbra is probably very nearly adiabatic, except for a thin superadiabatic layer just beneath the photosphere that we neglect here. There is no magnetic field in this layer since we assume that the penumbral magnetic field lies over the convection zone. The sound speed squared and local density scale height each increase linearly with depth in the lower layer, their functional forms being

$$c_2^2(z) = c_{20}^2 - g(\gamma_2 - 1)z \tag{4}$$

and

54

$$H_2(z) = H_{20} - (\gamma_2 - 1)z \quad . \tag{5}$$

The corresponding density distribution is

$$\rho_2(z) = \rho_{20}[1 - (\gamma_2 - 1)z/H_{20}]^{1/(\gamma_2 - 1)} \quad . \tag{6}$$

At the interface between the two layers (z=0), we require the undisturbed density to be continuous to avoid introducing interfacial gravity waves and wave reflections; therefore, $\rho_{10} = \rho_{20}$. In the unperturbed penumbra, there must be pressure equilibrium at the interface; that is, the gas pressure in the lower layer at z=0 must equal the sum of the gas pressure and the magnetic pressure in the upper layer at z=0. Therefore, the gas pressure is greater in layer 2 than in layer 1, and since the density is continuous across the interface, the temperature is greater in layer 2. This may be expressed in terms of the sound speeds and the Alfvén velocity at z=0 as

$$c_{20}^2 = \frac{\gamma_2}{\gamma_1} c_1^2 + \frac{\gamma_2}{2} v_0^2 \quad . \tag{7}$$

We now turn to the problem of computing eigenmodes of magneto-atmospheric waves in this penumbral model.

III. ANALYSIS

Consider first the behavior of small adiabatic perturbations in the lower layer (layer 2), an adiabatic atmosphere without magnetic field. Leibacher (1971) solved this problem in his study

55

of oscillations of the quiet photosphere. Here we take a slightly different approach than his, using other transformations which yield a different form of the propagation equation. For vanishing magnetic field ($\underline{B}_0 = \underline{B} = 0$), the vector equation for the perturbation velocity (equation (7), Paper I) becomes

$$\frac{\partial^2 \underline{u}_2}{\partial t^2} = c_2^2 \nabla\phi + (\gamma_2 - 1)\phi\underline{g} + \nabla(\underline{u}_2 \cdot \underline{g}) \quad , \tag{8}$$

where $\phi = \nabla \cdot \underline{u}_2$.

We assume that the perturbation velocity has the form $\underline{u}_2 = \hat{\underline{u}}_2(z) e^{i(k_x x - \omega t)}$, with propagation in the x-direction ($k_y = 0$). This implies that $\hat{v}_2 = 0$ and $\hat{\underline{u}}_2 = \hat{\underline{u}}_2(z) = (\hat{u}_2(z), 0, \hat{w}_2(z))$. All other perturbation quantities are represented in a similar manner, with a caret denoting the z-dependent amplitude in each case. From the two components of equation (8) and the definition of ϕ, we obtain the following relation:

$$\hat{w}_2(z) = \frac{g[\gamma_2 - c_2^2 k_x^2/\omega^2]\hat{\phi} - c_2^2 \frac{d\hat{\phi}}{dz}}{[\omega^2 - g^2 k_x^2/\omega^2]} \quad . \tag{9}$$

The pressure perturbation can also be written in terms of $\hat{\phi}$, using the continuity and energy relations (see Paper I):

$$\hat{p}_2 = -\frac{i\rho_2 c_2^2}{\omega} \left\{ \frac{[\omega^2 - g^2\gamma_2/c_2^2]\hat{\phi} + g\frac{d\hat{\phi}}{dz}}{[\omega^2 - g^2 k_x^2/\omega^2]} \right\} \quad . \tag{10}$$

Upon substitution of equation (9) into the z-component of equation (8), we obtain the following second-order differential equation for $\hat{\phi}$:

$$\frac{d^2\hat{\phi}}{dz^2} + \left[\frac{1}{c_2^2}\frac{dc_2^2}{dz} - \frac{g\gamma_2}{c_2^2}\right]\frac{d\hat{\phi}}{dz} + \left[\frac{\omega^2}{c_2^2} - k_x^2 + \frac{g^2 k_x^2}{\omega^2 c_2^2}(\gamma_2 - 1) + \frac{gk_x^2}{\omega^2 c_2^2}\frac{dc_2^2}{dz}\right]\hat{\phi} = 0 \ .$$

$$(11)$$

The nondimensional frequency, horizontal wavenumber, and depth, based on the values of sound speed and density scale height in layer 2 at $z=0$, are defined by

$$\Omega_2 \equiv \frac{H_{20}\omega}{c_{20}} \ , \qquad K_2 \equiv H_{20}k_x' \ , \qquad \text{and} \quad \tilde{z} \equiv \frac{z}{H_{20}} \ . \qquad (12)$$

By transforming the independent and dependent variables according to

$$Y = \frac{2K_2}{(\gamma_2 - 1)} - 2K_2\tilde{z} \ , \qquad \psi = e^{Y/2}\hat{\phi} \ , \qquad (13)$$

equation (11) assumes the form

$$Y\frac{d^2\psi}{dY^2} + (b-Y)\frac{d\psi}{dY} - a\psi = 0 \ , \qquad (14)$$

where

$$a = \frac{(2\gamma_2 - 1)}{2(\gamma_2 - 1)} - \frac{\Omega_2^2}{2K_2(\gamma_2 - 1)} \ , \qquad b = \frac{(2\gamma_2 - 1)}{(\gamma_2 - 1)} \ . \qquad (15)$$

Equation (14) is the standard form of Kummer's equation (see Abramowitz and Stegun 1964). The solutions of this equation are given in terms of Kummer's functions,

$$M(a,b;Y) = \frac{\Gamma(b)}{\Gamma(a)}\sum_{n=0}^{\infty}\frac{\Gamma(a+n)}{\Gamma(b+n)}\frac{Y^n}{n!} \ . \qquad (16)$$

The general solution of equation (14) is

$$\psi(Y) = D_3 M(a,b;Y) + D_4 U(a,b;Y) \ , \qquad (17)$$

57

where D_3 and D_4 are arbitrary constants and $U(a,b;Y)$ can be written in terms of Kummer's functions. To insure finite total perturbation energy, we must require that the vertical velocity of the perturbation vanish as $z \to -\infty$ or as $Y \to +\infty$. This in turn requires that $D_3 = 0$. The solution for $\hat{\phi}$ as a function of $\tilde{z}$ in the lower layer is then

$$\hat{\phi}(z) = D_4 \, \frac{\pi}{\sin\pi b} \, e^{-[\frac{K_2}{(\gamma_2-1)} \, - \, K_2\tilde{z}]} \left\{ \frac{M(a,b;\frac{2K_2}{(\gamma_2-1)} - 2K_2\tilde{z})}{\Gamma(1+a-b)\,\Gamma(b)} \, - \right.$$

$$\left. - \left[\frac{2K_2}{(\gamma_2-1)} - 2K_2\tilde{z} \right]^{1-b} \frac{M(1+a-b,2-b;\frac{2K_2}{(\gamma_2-1)} - 2K_2\tilde{z})}{\Gamma(a)\,\Gamma(2-b)} \right\} \, . \qquad (18)$$

The vertical velocity and pressure perturbation are given in terms of $\hat{\phi}$ by equations (9) and (10).

The form of the solution in the upper layer has been given in Paper I, and we shall not repeat the analysis here. The general form for the vertical velocity in the upper layer that gives finite total perturbation energy is given in terms of hypergeometric functions by either

$$\hat{w}_1(z) = D_1 e^{-\frac{zK_1}{H_1}} \, F(A,B;C; \frac{\Omega_1^2}{\beta^2(K_1^2-\Omega_1^2)} \, e^{-z/H_1}) \qquad (19)$$

for

$$\left| \frac{\Omega_1^2}{\beta^2(K_1^2-\Omega_1^2)} \right| < e^{z/H_1} \, , \qquad (20)$$

or else by

$$\hat{w}_1(z) = D_1 e^{-zK_1/H_1} \left\{ \frac{\Gamma(C)\,\Gamma(B-A)}{[\Gamma(B)]^2} \left[\frac{\beta^2(\Omega_1^2 - K_1^2)}{\Omega_1^2} \right]^A e^{zA/H_1} \quad \times \right.$$

$$F(A, 1-B; 1-B+A;\ \frac{\beta^2(K_1^2 - \Omega_1^2)}{\Omega_1^2}\ e^{z/H_1}) + \frac{\Gamma(C)\,\Gamma(A-B)}{[\Gamma(A)]^2} \left[\frac{\beta^2(\Omega_1^2 - K_1^2)}{\Omega_1^2} \right]^B e^{zB/H_1} \quad \times$$

$$\left. F(B, 1-A; 1-A+B; \frac{\beta^2(K_1^2 - \Omega_1^2)}{\Omega_1^2}\ e^{z/H_1}) \right\} \tag{21}$$

for

$$\left| \frac{\Omega_1^2}{\beta^2(K_1^2 - \Omega_1^2)} \right| > e^{z/H_1}\ . \tag{22}$$

Here

$$A + B = C = 2K_1 + 1\ , \tag{23}$$

$$AB = \Omega_1^2 + K_1 + \left(\frac{\gamma_1 - 1}{\gamma_1^2} \right) \frac{K_1^2}{\Omega_1^2}\ , \tag{24}$$

$$\beta^2 = v_0^2/c_1^2\ , \tag{25}$$

and Ω_1 and K_1 are nondimensional frequency and wavenumber defined as in (12), except scaling with c_1 and H_1.

The pressure perturbation in the upper layer consists of the sum of the gas pressure perturbation and the magnetic pressure perturbation. The gas pressure perturbation can be expressed in terms of the vertical velocity and its derivative as

$$\hat{p}_1 = -i\rho_1 c_1^2 \omega\ \frac{[\frac{d\hat{w}_1}{dz} - \frac{g}{c_1^2}\hat{w}_1]}{(\omega^2 - c_1^2 k_x^2)}\ . \tag{26}$$

The magnetic pressure perturbation $\hat{p}_m$ is found from the

59

linearization of

$$p_m + \hat{p}_m = \frac{(\underline{B}_0 + \hat{\underline{B}}) \cdot (\underline{B}_0 + \hat{\underline{B}})}{8\pi} \quad ,$$

where p_m is the unperturbed magnetic pressure. The components of the perturbed magnetic field are determined by the linearized induction equation (equation (4) of Paper I). We find

$$\hat{p}_m = -i \, \frac{v_A^2 \rho_1}{\omega} \, \frac{d\hat{w}_1}{dz} \tag{27}$$

The total perturbed pressure $\hat{p}_{T_1}$ in layer 1 is expressed in terms of the density and the Alfvén velocity as

$$\hat{p}_{T_1} = - \, \frac{i\rho_1}{\omega} \{ [(c_1^2 + v_A^2)\omega^2 - c_1^2 v_A^2 k_x^2] \frac{d\hat{w}_1}{dz} - \omega^2 g\hat{w}_1 \} / (\omega^2 - c_1^2 k_x^2) \quad . \tag{28}$$

IV. EIGENMODES AND RUNNING PENUMBRAL WAVES

We now have expressions for the vertical velocity and the pressure perturbation in each layer of the penumbral model, such that the total perturbation energy is finite. The remaining conditions are the matching of the vertical velocity and the perturbed pressure at the interface $z = 0$.

The scaling of frequency and wavenumber was done separately for each layer in order to simplify the propagation equation as much as possible in each case. In matching across the interface, we need the following relations between parameters in the two layers:

$$H_{20} = \gamma_2 (1 + \frac{\beta^2 \gamma_1}{2}) H_1 \quad , \tag{29}$$

60

$$\Omega_2^2 = \gamma_1 \gamma_2 \left(1 + \frac{\beta^2 \gamma_1}{2}\right) \Omega_1^2 \ , \tag{30}$$

$$K_2^2 = \gamma_2^2 \left(1 + \frac{\beta^2 \gamma_1}{2}\right)^2 K_1^2 \ , \tag{31}$$

and equation (7).

Continuity of the vertical velocity across z = 0 requires, after normalization, that

$$\hat{w}_1(0) = \hat{w}_2(0)' = 1 \ . \tag{32}$$

This condition fixes the values of the coefficients D_1 in equation (19) or (21) and D_4 in equation (18). The remaining condition, the continuity of the perturbed pressure, requires that we equate (10) and (28). This then leads to the nondimensional condition

$$\left\{ \frac{[(1+\beta^2)\Omega_1^2 - \beta^2 K_1^2]\frac{d\hat{w}_1}{d\hat{z}_1}\Big|_0 - \frac{\Omega_1^2}{\gamma_1}\hat{w}_1(0)}{(\Omega_1^2 - K_1^2)} \right\} = \frac{1}{\gamma_1} \left\{ \frac{\Omega_2 \gamma_2 \tilde{\phi}(0) + \frac{d\tilde{\phi}}{d\hat{z}_2}\Big|_0}{(\Omega_2^2 - K_2^2/\Omega_2^2)} \right\} \ , \tag{33}$$

where $\tilde{\phi} = \hat{\phi} H_{20}$. Equation (33) is only satisfied by particular values of frequency and wavenumber, and gives the dispersion relation for eigenmodes of oscillation in the penumbral model.

In order to evaluate the dispersion relation (33), the free parameters β^2, γ_1, and γ_2 must be specified, which then effectively determines the properties of the model. Although it is possible to evaluate (33) for different values of γ in each layer (for example, a lower value of γ_1 could be taken to represent radiative transfer in the upper layer), we chose the usual value of 5/3 for both layers. The dispersion relation (33) was solved numerically by inserting values of K_1 and then computing and comparing the two

61

sides of (33) for small increments in Ω_1.

Figure 2 shows the first several eigenmodes of the two-layer penumbral model for $\beta^2 = 0.5$ and $\gamma_1 = \gamma_2 = 5/3$. The value of β^2 was chosen to represent a typical penumbra and is slightly less than the value of β^2 at $z = 0$ in our earlier penumbral model (NT). Here we have classified the eigenmodes as "plus" or "minus" modes, following the terminology used in the case of an atmosphere with constant sound speed, density scale height, and Alfvén velocity (see McLellan and Winterberg 1968 and NT). The plus modes all lie above the upper dashed line $\Omega = K$ in figure 2, which corresponds to $\omega = c_1 k_x$ (the Lamb mode). The minus mode (there is only one in this case) lies below the lower dashed line $\Omega = \beta K$ which corresponds to $\omega = v_0 k_x$. There are no eigenmodes in the region between the dashed lines. This classification of plus or minus modes refers here to the character of the eigenmode in the upper layer; in the lower layer, all of the modes have the character of acoustic waves (no magnetic field and no buoyancy).

Observational data on penumbral waves are included in figure 2 for comparison. The most commonly reported observational quantities are the period and the horizontal phase velocity, although they are not always measured simultaneously. Giovanelli (1974) reports a typical phase velocity of running penumbral waves of 15 km s^{-1} and typical periods in the range of 180-240 s. He did report phase velocities of up to 21 km s^{-1}, however, and gave specific periods and wavelengths for four sunspots (denoted by

62

crosses in figure 2). The data of Beckers and Schultz (1972) appear to indicate a penumbral oscillation period of 255 s. Moore and Tang (1975) observed penumbral waves with period 270 ± 10 s in a single sunspot. Zirin and Stein (1972) state that the periods of penumbral waves in twenty sunspots were almost all between 240 s and 300 s, and the measured horizontal phase velocity of 9.4 km s^{-1} in one spot was more or less the same in other spots even when the period varied.

The quadrangle in figure 2 represents the range of observations: periods from 180 s to 300 s, and phase velocities from 9.4 km s^{-1} to 21 km s^{-1}, with a dashed line at 15 km s^{-1} to indicate the value that Giovanelli considers typical. The first plus mode of the penumbral model passes through this quadrangle. Although the particular eigenmode of oscillation of the penumbra is determined by the excitation, and little is known about the excitation, the present results indicate that it is the first plus eigenmode that is being excited. This agrees with our earlier conclusions (NT).

The value $\beta^2 = 0.5$ used in figure 2 was chosen to represent a typical penumbra. In figure 3 the effect of changes in β^2 on the first plus mode is shown for a range of β^2 of two orders of magnitude (0.05, 0.5, 5.0). This constitutes a reasonable set of limits on β^2 for penumbral conditions, and is obtained by looking at the normal variation of B (factor of 4), ρ (factor of 4), and c^2 (factor of 1.5) expected in different penumbrae. We see that for any reasonable value of β^2, the penumbral model

63

has a first plus mode within the range of observations.

The vertical distributions of velocity and kinetic energy of the first plus mode (for $\beta^2 = 0.5$) are shown in figure 4 for $K_1 = 0.1995$ and $\Omega_1 = 0.3628$, corresponding to a horizontal wavelength $\lambda = 3,000$ km and period $\tau = 250$ s for $c_1^2 = 43.5$ km^{2}s^{-2}. Here the nondimensional height is scaled everywhere by the density scale height in the upper layer, H_1. The velocity distribution is fairly symmetric with the maximum amplitude occurring slightly above $z = 0$ in the penumbral photosphere. The kinetic energy, on the other hand, is almost entirely trapped in the lower layer (convection zone) with maximum energy just below the interface. The velocity amplitude decays slowly with height with a value of more than 25% of the maximum amplitude at a distance of eight scale heights above the level of that maximum.

There is a discrepancy between the height of maximum velocity predicted here ($z \sim 100$ km) and that predicted in our earlier paper (NT, $z \sim 1000$ km). Here the Alfvén velocity increases exponentially with height above the photosphere, whereas in NT it increased linearly. Thus, the downward refraction of waves is much stronger in the present model. The actual situation is probably somewhere between these two cases. In either case, the wave energy lies mostly below the height of maximum vertical velocity, in the convection zone and low photosphere.

64

V. CONCLUSIONS

The present results, taken together with our earlier work
(NT), indicate that running penumbral waves should be identified
with the lowest plus mode of trapped magneto-atmospheric waves
in the penumbra. The vertical trapping is primarily due to the
increasing Alfvén velocity up into the chromosphere and the in-
creasing sound speed down into the convection zone. Most of
the energy of the penumbral waves lies in the convection zone
and low photosphere, at the same level as the expected source
of excitation (umbral oscillatory convection). The maximum wave
amplitude occurs somewhat higher.

The results also indicate that penumbral waves should be
observable in a photospheric spectral line (see figure 4) as
well as in Hα. There is some indication of this in the obser-
vation of Beckers and Schultz (1972). Their data show a 255 s
period oscillation in the penumbra of one sunspot observed in
a photospheric line. They present contours of vertical velocity
as a function of horizontal position and time (their figure 1)
in which one may note horizontal propagation outward across
the penumbra at about the right phase speed. We plan further
observations in a search for penumbral waves in the photosphere.

Acknowledgements

REFERENCES

Abramowitz, M., and Stegun, I. A. (ed.), 1964, Handbook of
    Mathematical Functions, National Bureau of Standards,
    Washington, D. C., p. 503.

Beckers, J. M., and Schultz, R. B. 1972, Solar Phys. 27, 61.

Bray, R. J., and Loughhead, R. E. 1964, Sunspots, Chapman and
    Hall, London, 212.

Giovanelli, R. G. 1972, Solar Phys. 27, 71.

Giovanelli, R. G. 1974, in R. Grant Athay (ed.), "Chromospheric
    Fine Structure", I.A.U. Symp. 56, 137.

Leibacher, J. W. 1971, Ph.D. Thesis, Harvard University.

McLellan, A., and Winterberg, F. 1968, Solar Phys. 4, 401.

Moore, R. L. 1973, Solar Phys. 30, 403.

Moore, R. L., and Tang, F. 1975, Solar Phys. 41, 81.

Nishi, K., and Makita, M. 1973, Publ. Astron. Soc. Japan 25, 51.

Nye, A. H., and Thomas, J. H. 1974, Solar Phys. 38, 399.

Nye, A. H., and Thomas, J. H. 1975, Astrophys. J.

Zirin, H., and Stein, A. 1972, Astrophys. J. 173, L85.

FIGURE CAPTIONS

Fig. 1   Distribution of c^2 and v_A^2 with height z in the two-
          layer penumbral model. The upper layer (1) is iso-
          thermal with a uniform horizontal magnetic field.
          The lower layer (2) has an adiabatic temperature
          gradient and no magnetic field.

Fig. 2   The first five plus eigenmodes and the only minus
          eigenmode of the two-layer penumbral model for $\beta^2 = 0.5$,
          $\gamma_1 = \gamma_2 = 5/3$. The quadrangle represents the range of
          observational data (see text). The crosses correspond
          to particular observations (Giovanelli 1974).

Fig. 3   The first plus eigenmode evaluated for extreme values
          of β^2 for sunspot penumbrae (see text): $\beta^2_{max} = 5.0$,
          $\beta^2_{min} = 0.05$. The quadrangle represents the range of
          observational data. The crosses correspond to
          particular observations (Giovanelli 1974).

Fig. 4   The distribution of vertical velocity and kinetic energy
          of the first plus eigenmode with nondimensional height
          z/H_1. The velocity and energy are each normalized to
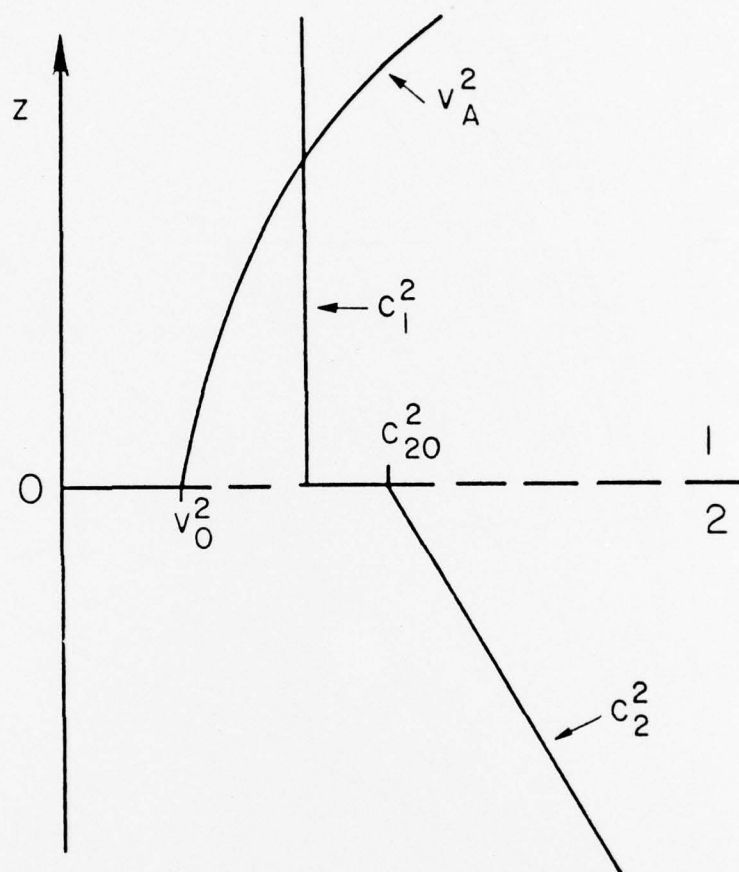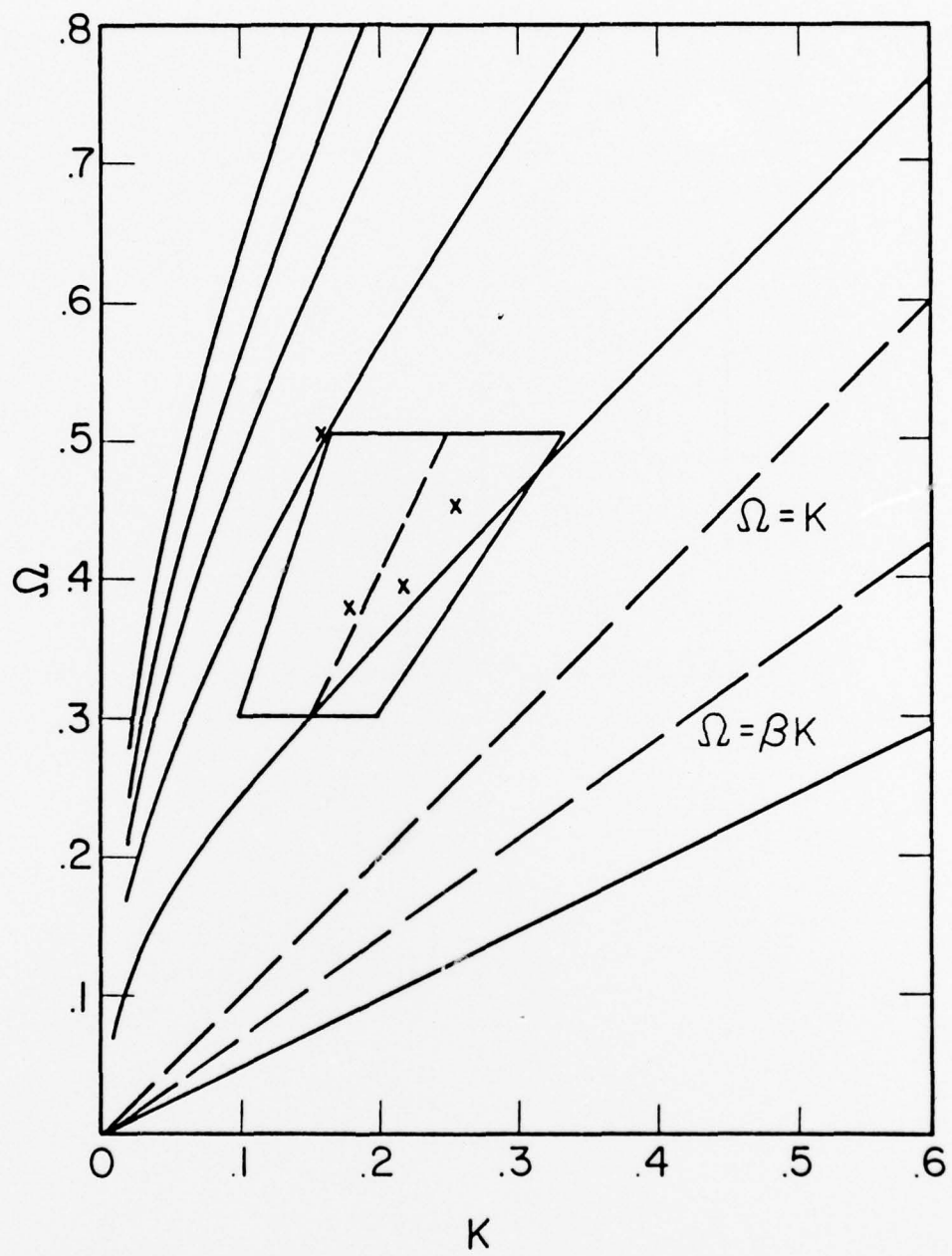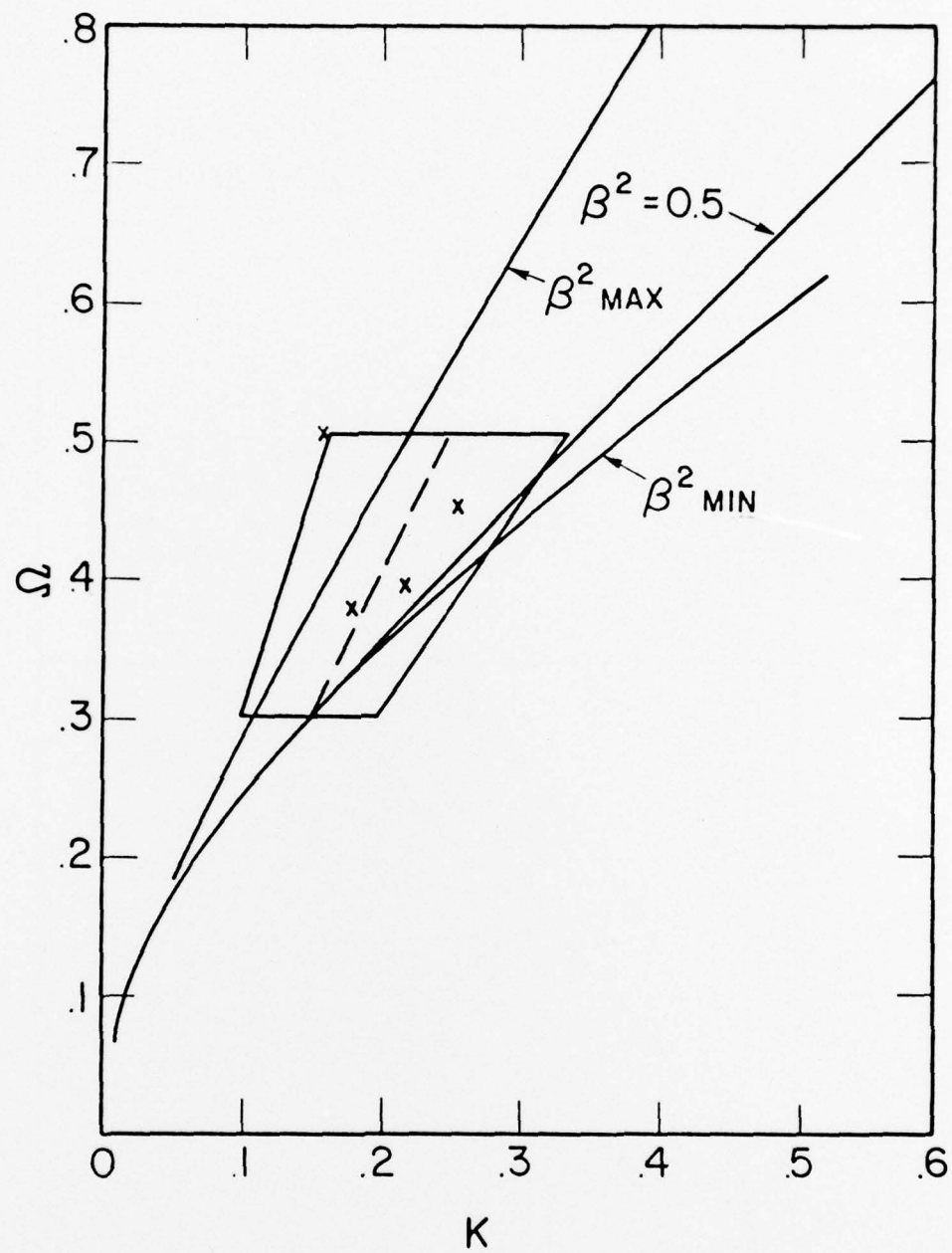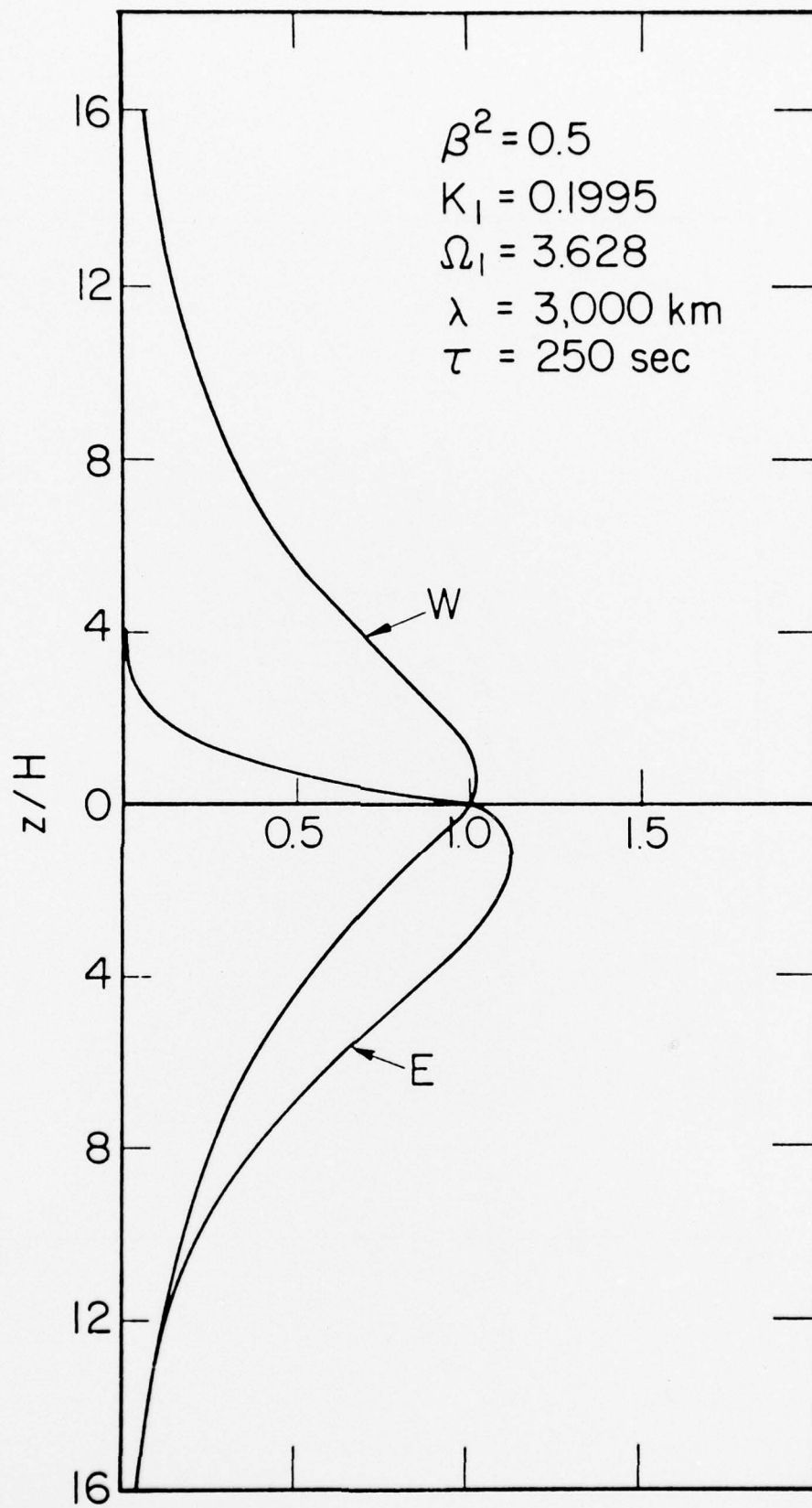   value unity at the interface $z/H_1 = 0$.

68

Fig. 1

Fig. 2

70

Fig. 3

71

$\beta^2 = 0.5$
$K_1 = 0.1995$
$\Omega_1 = 3.628$
$\lambda = 3,000$ km
$\tau = 250$ sec

Fig. 4

72